New Phytologist

Research

Aridity drove the evolution of extreme embolism resistance and the radiation of conifer genus *Callitris*

Maximilian Larter[1], Sebastian Pfautsch[2], Jean-Christophe Domec[3,4], Santiago Trueba[5,6], Nathalie Nagalingum[7] and Sylvain Delzon[1]

[1]BIOGECO, INRA, Univ. Bordeaux, Pessac 33610, France; [2]Hawkesbury Institute for the Environment, Western Sydney University, Locked Bag 1797, Penrith, NSW 2751, Australia; [3]Bordeaux Sciences AGRO, UMR 1391 ISPA INRA, 1 Cours du Général de Gaulle, Gradignan Cedex 33175, France; [4]Nicholas School of the Environment, Duke University, Durham, NC 27708, USA; [5]Department of Ecology and Evolutionary Biology, University of California, Los Angeles, UCLA, 621 Charles E. Young Dr. South, Los Angeles, CA 90095, USA; [6]IRD, UMR AMAP, BPA5, Noumea 98800, New Caledonia; [7]National Herbarium of New South Wales, Royal Botanic Gardens & Domain Trust, Mrs Macquaries Rd, Sydney, NSW 2000, Australia

Author for correspondence:
Maximilian Larter
Tel: +33 6 79 70 92 75
Email: maximilien.larter@gmail.com

Received: *30 December 2016*
Accepted: *26 February 2017*

New Phytologist (2017)
doi: 10.1111/nph.14545

Key words: climate change, diversification, drought, ecophysiology, embolism resistance, evolution, gymnosperms, xylem.

Summary

• Xylem vulnerability to embolism is emerging as a major factor in drought-induced tree mortality events across the globe. However, we lack understanding of how and to what extent climate has shaped vascular properties or functions. We investigated the evolution of xylem hydraulic function and diversification patterns in Australia's most successful gymnosperm clade, *Callitris*, the world's most drought-resistant conifers.

• For all 23 species in this group, we measured embolism resistance (P_{50}), xylem specific hydraulic conductivity (K_s), wood density, and tracheary element size from natural populations. We investigated whether hydraulic traits variation linked with climate and the diversification of this clade using a time-calibrated phylogeny.

• Embolism resistance varied widely across the *Callitris* clade (P_{50}: −3.8 to −18.8 MPa), and was significantly related to water scarcity, as was tracheid diameter. We found no evidence of a safety-efficiency tradeoff; K_s and wood density were not related to rainfall. *Callitris* diversification coincides with the onset of aridity in Australia since the early Oligocene.

• Our results highlight the evolutionary lability of xylem traits with climate, and the leading role of aridity in the diversification of conifers. The uncoupling of safety from other xylem functions allowed *Callitris* to evolve extreme embolism resistance and diversify into xeric environments.

Introduction

In the light of current climate change, the role of environmental fluctuation in driving biodiversity and its distribution is of particular interest (Thuiller *et al.*, 2005, 2011). It is now clear that rapid and pronounced changes in environmental conditions can: reduce climatic niche availability, potentially driving populations or species to extinction (Mittelbach *et al.*, 2007; Eiserhardt *et al.*, 2015); open up new suitable niche space allowing range expansion; drive adaptation; and even lead to the emergence of new species (Pennington *et al.*, 2004; Hua & Wiens, 2013; Koenen *et al.*, 2015; Qvarnström *et al.*, 2016). For example, the transition to a colder and drier climate in the mid-to-late Miocene (*c.* 13.8–5.3 million yr ago (Ma)) is associated with vegetation changes in the Cape Flora of South Africa, leading to a major increase in diversification in Aizoaceae (Dupont *et al.*, 2011). Over the same period, the South American orchid genus *Hoffmannseggella* radiated into more open habitats with the cooling climate in eastern Brazil (Antonelli *et al.*, 2010). The emergence of the sclerophyll biomes in Australia 25 Ma has also been associated with adaptive radiations, with evidence from the fossil record (Carpenter *et al.*, 1994; Hill, 2004) and using phylogenetics, for example, in *Banksia* and eucalypts (Crisp *et al.*, 2004). Although we do not fully understand the rise of the angiosperms (Augusto *et al.*, 2014), climate shifts at the end of the Eocene *c.* 34 Ma could also explain the decline of some gymnosperm lineages (Crisp & Cook, 2011).

Although some species have shown great capacity for adaptation (Meyers & Bull, 2002) and shifts in distribution (Davis & Shaw, 2001), reports of potential habitat contraction and increasing extinction risk of tree species as a consequence of today's rapid climate change are increasing (e.g. Eiserhardt *et al.*, 2015; Corlett & Westcott, 2013; Sax *et al.*, 2013). It thus becomes apparent that in order to better predict climate change-induced effects on diversity and habitat range of trees, it is necessary to identify adaptive traits that could offer resistance to extinction and have the potential to respond to natural selection during rapid climate change.

For vascular plants, and tall trees in particular, providing a continuous stream of water to their photosynthetic aerial shoots

is one of their most vital needs and greatest challenges, especially as climate change will increase frequency and severity of droughts and heat waves (Stocker *et al.*, 2013; Pfautsch, 2016). Water transport in plants is driven by the process of transpiration at the leaf–atmosphere interface, which generates a water-potential gradient throughout the plant. Formalized by the cohesion-tension theory (Dixon, 1914; Tyree & Zimmermann, 2002), water transport is possible thanks to the strong hydrogen bonds between water molecules that allow liquid water to remain in a metastable state while at negative pressure, i.e. under tension. The main drawback of this remarkable function is the risk of xylem embolism, or breakage of the water column because of cavitation, which becomes ever more likely as evaporative demand increases, and as soil water potential declines during drought. After embolism, the air-filled conduits restrict water transport, and high amounts of xylem embolism can lead to plant death (Brodribb & Cochard, 2009; Urli *et al.*, 2013). The breakdown of the vascular system through embolism is thought to be involved in multiple mass mortality events during and after droughts in forests across the globe in recent decades (Anderegg *et al.*, 2012, 2016). Various adaptive mechanisms protect plants from these potentially catastrophic events, such as limiting water loss through transpiration and the drop in xylem pressure by closing stomata early during drought (Delzon & Cochard, 2014), or xylem adaptations that limit the formation of air bubbles and the irreversible spread of embolism (Schuldt *et al.*, 2015; Lübbe *et al.*, 2016). Recent advances have revealed that cavitation events occur at air–sap interfaces within pores between functional and embolized conduits (Choat *et al.*, 2008; Lens *et al.*, 2013). In conifers, bordered pits contain a valve-like structure called the torus which is deflected to block the pit aperture, protecting functional tracheids from air entry (Bailey, 1916). While this provides conifers with increased protection from embolism compared with angiosperms (Maherali *et al.*, 2004; Pittermann *et al.*, 2005; Choat *et al.*, 2012), embolism still occurs as a result of imperfect sealing of the pit aperture by the torus (Bouche *et al.*, 2014).

Plants need to balance embolism resistance (xylem safety) with optimizing rates of water transport (xylem efficiency) to their photosynthetic organs (Tyree & Zimmermann, 2002; Hacke *et al.*, 2006). The advantages of xylem safety are evident (i.e. increased survival during drought), whereas xylem efficiency allows increased carbon allocation to leaves relative to sapwood area, for example, allowing rapid growth and optimizing photosynthesis in competitive settings (Santiago *et al.*, 2004; Poorter *et al.*, 2010). The link between safety and efficiency is indirect, as wider conductive elements transport water efficiently but are weaker under the mechanical stress imposed by negative xylem pressure in drought-tolerant species (Sperry *et al.*, 2008). Thicker cell walls could influence pit morphology, notably the pit membrane, thereby increasing xylem embolism resistance (Tyree & Sperry, 1989; Li *et al.*, 2016). The final compromise reached between safety and efficiency is strongly determined by species ecology and phylogeny. For example, species growing in competitive wet environments are more likely to maximize efficiency over safety (Sperry *et al.*, 2006; Choat *et al.*, 2012). In any case, there is little evidence of a universal and strong relationship between safety and efficiency at a higher ecological and taxonomic scale. This tradeoff is only suggested by the absence of species with a xylem that combines both embolism resistance and transport efficiency (Gleason *et al.*, 2016). However, there are many 'incompetent' species, i.e. with vasculature that is both vulnerable to embolism and inefficient for water transport. The impact of water availability on water transport efficiency seems, however, to be noticeable at more restricted evolutionary scales. For instance, xeric *Eucalyptus* species evolved narrower vessels and denser wood than species in more mesic environments, reflecting a tradeoff of hydraulic traits in response to climate across Australia (Pfautsch *et al.*, 2016). Similarly, tracheid lumen diameter tracks rainfall across *Callitris columellaris* populations (Bowman *et al.*, 2011).

At broad evolutionary scales there is substantial variation in the xylem pressure inducing 50% loss of hydraulic conductance, termed P_{50} (Maherali *et al.*, 2004; Pittermann *et al.*, 2012; Bouche *et al.*, 2014). On the other hand, at finer infrageneric and intraspecific scales there is generally low variability (Delzon *et al.*, 2010) and little genetic differentiation for xylem embolism resistance (Lamy *et al.*, 2011; Sáenz-Romero *et al.*, 2013; but see David-Schwartz *et al.*, 2016; Hajek *et al.*, 2016). However, no studies have examined embolism resistance among closely related species over a wide climatic gradient. *Callitris* is a conifer genus of shrubs and trees that underwent an ecological radiation with the emergence of dry environments in Australia over the last 30 million yr (Pittermann *et al.*, 2012). It is the largest genus of Cupressaceae in the southern hemisphere, with 15–20 species recognized by different authors (Hill & Brodribb, 1999; Farjon, 2005; Eckenwalder, 2009; Piggin & Bruhl, 2010). This clade displays a marked xeric affinity, despite spanning a huge rainfall gradient across Australia and New Caledonia, i.e. from *c.* 200 to over 2000 mm yr^{-1}. With some of the most drought-tolerant species currently known (Brodribb *et al.*, 2010; Larter *et al.*, 2015), this clade presents an ideal group of species to investigate plant ecophysiology and the development of drought tolerance from an evolutionary perspective.

Our main objective was to investigate the evolution of the vascular system of all members of the *Callitris* clade. First, we constructed an extensive physiological dataset of xylem embolism resistance, xylem specific hydraulic conductivity and xylem anatomical traits. We then obtained species occurrence data and tested whether variation in hydraulic traits was linked to species climatic preferences and the diversification of this clade, established with a time-calibrated phylogeny based on DNA sequence data from multiple loci. We hypothesized that, owing to the large aridity gradient occupied by this clade, resistance to embolism should vary widely and track climatic conditions. Given the genus-level phylogenetic scale and extensive climatic gradient, our second hypothesis was that a tradeoff existed between safety and hydraulic efficiency, as a result of large selective pressures from competition and climatic stress driving hydraulic traits. Specifically, we expected the most xeric species to have a resistant, less efficient xylem with many narrow tracheids, while species from more mesic regions would have wider tracheids, favoring

xylem efficiency but reducing safety from embolism. Our third hypothesis was that if hydraulic traits in this group evolved rapidly in response to climate, then phylogeny would have little impact on traits and tradeoffs. In relation to this hypothesis, we expected that the distribution of members of the *Callitris* clade reflected an ecological radiation in response to increasing aridity in the Australian region since the end of the Eocene *c.* 34 Ma.

Materials and Methods

Collection of plant materials

For the purpose of this study, we collected samples from wild populations for *Actinostrobus acuminatus*, *Actinostrobus arenarius*, *Actinostrobus pyramidalis*, *Callitris canescens*, *Callitris drummondii*, *Callitris endlicheri*, *Callitris glaucophylla*, *Callitris gracilis*, *Callitris muelleri*, *Callitris neocaledonica*, *Callitris roei*, *Callitris sulcata*, *Callitris verrucosa*, and *Neocallitropsis pancheri* and from botanical gardens for *Callitris baileyi*, *Callitris endlicheri*, *Callitris macleayana*, and *Callitris monticola* (Table 1; Fig. 1). We also included data from previous studies for *Callitris tuberculata*, *C. columellaris*, *C. gracilis*, *Callitris preissii*, *Callitris rhomboidea* and *A. pyramidalis* (Brodribb *et al.*, 2010; Delzon *et al.*, 2010; Larter *et al.*, 2015), and pooled data from all sources for analysis. The close relationship between the genera *Callitris* s.s., *Neocallitropsis* and *Actinostrobus* (Pye *et al.*, 2003; Piggin & Bruhl, 2010) led us to treat them as a single *Callitris* clade (or *Callitris* s.l.). We collected straight branches *c.* 40 cm long and 1 cm in diameter, using hand-held secateurs or telescopic branch-cutters from sun-exposed parts of the crown, although we expect little variation in xylem embolism resistance across organs in conifers (Bouche *et al.*, 2016). We sampled three to 10 individuals depending on the availability of healthy adult trees. We immediately removed all leaves on the branches, and carefully wrapped the samples (in wet paper towels, plastic bags and packing tape), to avoid any water loss during courier transport to analytical facilities in Bordeaux, France. They were then shipped as quickly as possible, refrigerated and maintained in a humid environment until hydraulic measurements were conducted.

Species climate

The climate experienced by *Callitris* species varies widely from hot, semiarid Mediterranean climate in southwestern and central Australia to wet tropical or monsoonal climates in Northern Australia, Queensland and New Caledonia (Fig. 1). In order to describe each species' climate, we downloaded species occurrence points from the Global Biodiversity Information Facility (GBIF; Booth, 2014). After excluding data with possible species misidentification or GPS coordinate errors, we extracted climate information for each point using climate data from the WorldClim database (Hijmans *et al.*, 2005) using QGIS software (Quantum, 2011). We also obtained potential evapotranspiration (P-ET) and aridity index (AI) from the CGIAR-CSI database (Trabucco & Zomer, 2009). We then extracted the mean and median values of the distributions of each climatic variable for each species.

Physiological and anatomical traits

All hydraulic measurements were done with the standard protocol developed at the University of Bordeaux using the 'Cavitron' technique (Cochard *et al.*, 2005), which uses centrifugal force to induce a negative pressure in a spinning sample. The loss of hydraulic conductance as a result of embolism is monitored while incrementally decreasing the negative pressure experienced in the xylem. We used a thicker, reinforced rotor specifically designed to safely reach high speeds (26 000 ***g***, or 13 000 rpm with a standard 27.5 cm rotor), inducing xylem pressure below −16 MPa. This technique allowed us to construct vulnerability curves and simultaneously estimate xylem specific hydraulic conductivity K_s ($kg\,m^{-1}\,MPa^{-1}\,s^{-1}$), derived from the maximum conductance measured at high xylem pressure divided by sample length and sapwood area. A sigmoid model was fitted to each individual vulnerability curve (207 in total) from which we obtained the P_{50} parameter (MPa), which is the xylem pressure inducing 50% loss of conductance (Pammenter & Vander Willigen, 1998). Values were then averaged across all samples for each species.

Following xylem embolism resistance measurements, a 1–2 cm segment was excised from the basal part of the samples in order to conduct xylem anatomy measurements. Several transverse sections per individual were cut using a sliding microtome, stained using safranine at 1%, and examined using a light microscope (DM2500M; Leica Microsystems, Wetzlar, Germany). We selected three individuals per species and took five digital images per individual, which were then analyzed using ImageJ (NIH, Bethesda, MD, USA). Magnification was ×400 for all samples except for *N. pancheri*, *C. sulcata* and *C. neocaledonica*, for which we used ×200 magnification to increase the total number of tracheids visible on each image. Sample preparation and photography were conducted at either the University of Bordeaux or Western Sydney University (Hawkesbury Institute for the Environment), using the same protocol. Images were manually edited to remove imperfections before automatic image analysis. Tracheids with an incomplete lumen (i.e. placed on the edge of the images) were excluded from the analysis. Overall, 80 individual samples (three to five per species) and a total of 400 images were analyzed, resulting in a total of 33 652 tracheids measured. We extracted from each image the area of each tracheid lumen, total image area and number of analyzed tracheids, and pooled the data by individual for analysis. From the total analyzed area, total tracheid number, and area of each tracheid, we derived for each individual mean, minimum and maximum tracheid diameter, the average number of tracheid per unit area (TF; $n\,mm^{-2}$) and the ratio of tracheid lumen area divided by total image area (void to wood ratio; %).

According to the Hagen–Poiseuille law, hydraulic conductivity of a conduit varies according to the fourth power of its diameter, which means that larger tracheids contribute disproportionately more to the overall hydraulic conductance (Tyree & Zimmermann, 2002). To use a hydraulically meaningful measure of tracheid diameter, we calculated the hydraulically weighted hydraulic diameter (D_h; Tyree & Zimmermann, 2002), defined as:

New Phytologist (2017)
www.newphytologist.com

Table 1 Sampling details for all species in this study (natural populations and botanic gardens locations) and median values for aridity index (AI), mean annual temperature (MAT) and mean annual precipitation (MAP) of each species' distribution

Species	Authority	*N*	Natural population location	Latitude	Longitude	Elevation (m)	Botanic garden location	Latitude	Longitude	Elevation (m)	AI	MAT	MAP	Reference[2]
Actinostrobus acuminatus	*Parl.*	10	Western Australia	−30.494 28	115.422 53	195					0.39	18.5	576	
Actinostrobus arenarius	*C.A.Gardner*	11	Western Australia	−30.861 39	116.721 67	338	Mt Annan BG, NSW, Aus.	−34.06984	150.764 94	155	0.26	19.15	408.5	
Actinostrobus pyramidalis	*Miq.*	12	Western Australia	−30.627 31	115.941 36	204					0.48	18.2	698	1
Callitris baileyi	*C.T.White*	3					Mt Annan BG, NSW, Aus.	−34.06984	150.764 94	155	0.59	18.1	878	
Callitris canescens[1]	*(Parl.) S.T.Blake*	10	Western Australia	−33.110 78	118.354 28	305	Mt Annan BG, NSW, Aus.	−34.06984	150.764 94	155	0.28	16.5	372	
		10	South Australia	−34.999 25	139.555 33	77								
Callitris columellaris	*F.Muell.*	3									0.22	19.6	367	2
Callitris drummondii	*(Parl.) Benth. & Hook.f. ex F.Muell.*	13	Western Australia	−33.678 81	120.185 61	134					0.37	16.6	495	
Callitris endlicheri	*F.M.Bailey*	9	New South Wales	−33.137 00	150.074 61	612					0.49	15.7	696	
Callitris glaucophylla	*J.Thomps. & L.A.S.Johnson*	13	New South Wales	−32.434 81	149.846 19	707	Mt Annan BG, NSW, Aus.	−34.06984	150.764 94	155	0.32	17.2	459	
Callitris gracilis	*R.T.Baker*	8	South Australia	−34.072 93	140.798 88	57					0.32	15.8	421	2
Callitris intratropica	*R.T.Baker & H.G.Sm.*	5					Royal BG Sydney, NSW, Aus.	−33.86557	151.214 15	30	0.69	26.8	1232.5	
Callitris macleayana	*(F.Muell.) F. Muell.*	3					Mt Annan BG, NSW, Aus.	−34.06984	150.764 94	155	1.32	17.7	1690	
Callitris monticola	*J.Garden*	7					Mt Tomah BG, NSW, Aus.	−33.53942	150.419 62	950	0.94	14.25	1220	
Callitris muelleri	*(Parl.) Benth. & Hook.f. ex F.Muell.*	8	New South Wales	−33.732 42	150.371 92	815					1.07	13.9	1233	
Callitris neocaledonica	*Dümmer*	11	New Caledonia	−21.882 50	166.416 39	1391					2.03	18.3	2320	
Callitris oblonga	*Rich. & A.Rich*	4					Royal BG Kew, UK	51.43539	−0.751 73	53	0.8	12.8	918	
Callitris preissii	*Miq.*	3									0.26	17	363	2

Table 1 Continued.

Species	Authority	*N*	Natural population location	Latitude	Longitude	Elevation (m)	Botanic garden location	Latitude	Longitude	Elevation (m)	AI	MAT	MAP	Reference[2]
Callitris rhomboidea	*R.Br. ex Rich. & A.Rich.*	8									0.83	14.6	924	1, 2
Callitris roei	*(Endl.) F.Muell.*	9	Western Australia	−33.108 06	118.334 39	346					0.29	16.2	387	
Callitris sulcata	*(Parl.) Schltr.*	9	New Caledonia	−22.133 65	166.488 87	16					0.98	22.5	1252	
Callitris tuberculata	*R.Br. ex R.T.Baker & H.G.Sm.*	11	Western Australia	−33.110 78	118.354 28	305	Mt Annan BG, NSW, Aus.	−34.06984	150.764 94	155	0.21	17.3	304	3
Callitris verrucosa	*(A.Cunn. ex Endl.) R.Br. ex Mirb.*	9	South Australia	−35.018 28	139.465 61	71					0.25	16.3	345	
Neocallitropsis pancheri	*(Carrière) de Laub.*	18	New Caledonia	−22.231 94444	166.860 5556	244					1.79	21.5	2162	

[1]*C. canescens* was sampled from two wild populations, in Western Australia and South Australia, as well as one individual from Mt Annan BG, NSW.
[2]References for data taken from previous studies: 1, Delzon *et al.* (2010); 2, Brodribb *et al.* (2010); 3, Larter *et al.* (2015).

$$D_h = \left[\frac{\sum D^4}{N}\right]^{1/4} \quad \text{Eqn 1}$$

where N is the total number of tracheids and D_h is the mean diameter required to achieve the same overall conductance with the same number of conductive elements. We then calculated the theoretical conductance (K_{th}; kg m^{-1} MPa^{-1} s^{-1}), which is the theoretical rate of flow through a cylindrical pipe according to the Hagen–Poiseuille law:

$$K_{th} = \frac{D_h^4 \pi \rho}{128 * \eta} * \mathrm{TF} \quad \text{Eqn 2}$$

where η is the viscosity of water at 20°C (1.002×10^{-9} MPa s) and ρ is the density of water at 20°C (998.2 kg m^{-3}). For appropriate units, we transformed D_h to m ($\times 10^{-6}$) and TF to m^{-2} ($\times 10^{5}$).

Xylem water flow efficiency represents the joint conductivity of both tracheid lumens (i.e. K_{th}) and bordered pits (Hacke *et al.*, 2005). We calculated pit conductivity K_{pit} (kg m^{-1} MPa^{-1} s^{-1}) as follows:

$$K_{pit} = \left(\frac{1}{K_s} - \frac{1}{K_{th}}\right)^{-1} \quad \text{Eqn 3}$$

We macerated sapwood of 14 *Callitris* species and measured length (μm) and counted bordered pits (hereafter pitting) of 700 individual tracheids (50 per species), for a subset of species representative of the range of climate encountered by *Callitris*. To prepare maceration slides (after Franklin, 1945), splinters of outer sapwood were incubated for 12 h at 60°C in plastic vials (2 ml Eppendorf) that contained acetic acid and hydrogen peroxide (50 : 50). Following the incubation, splinters were repeatedly washed and dehydrated in ethanol (50–70–96%) with water before staining with safranin–ethanol solution. After excess stain was removed, samples were mounted on glass slides, and cells were imaged using a light microscope and a digital camera (Leica DFC 500); ImageJ was again used for image analysis.

Wood density was estimated using X-ray imagery (Polge, 1966) for three individuals per species on transversal sections of *c.* 1 mm thickness. We used a silicone scale of known densities for calibration, and analyzed the images using Windendro (Guay *et al.*, 1992) to obtain two radial density profiles per section, from which we estimated mean wood density (g cm^{-3}).

Phylogenetic reconstruction

We built on the increased availability of molecular sequences to produce a new phylogeny of *Callitris*, *Actinostrobus* and *Neocallitropsis*. We took a broad view of species delimitations, i.e. treating *C. columellaris*, *Callitris intratropica*, and *C. glaucophylla* separately, as well as *C. tuberculata*, *C. preissii*, *C. verrucosa* and *C. gracilis*. Various treatments of these as subspecies and/or synonyms are available in the literature (Hill, 1998; Hill & Brodribb, 1999; Farjon, 2005, 2010; Eckenwalder, 2009). We

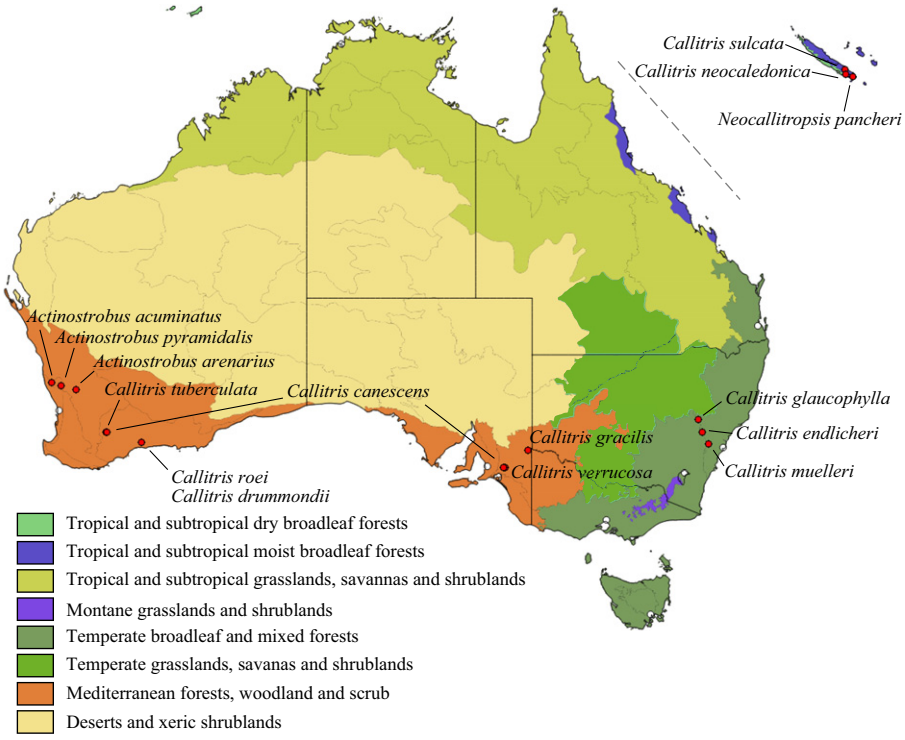

Fig. 1 Map of locations of wild populations sampled for this study. Colors represent terrestrial eco-regions taken from Olson *et al.* (2001).

used the PHLAWD pipeline (Smith *et al.*, 2009) to obtain sequences from GenBank (Benson *et al.*, 2011) with the aim of constructing a large multilocus dataset. We used a range of loci from plastid (rbcL, matK, trnL, psbB, petB) and nuclear DNA (ITS, needly, leafy). To complete the dataset, we used unpublished sequences (rbcL and matK) for the species *C. roei*, *C. monticola*, *C. baileyi*, and *C. columellaris* (N. Nagalingum, pers. comm.).

Alignments from PHLAWD were manually trimmed and checked, and we selected the most appropriate DNA substitution models using maximum likelihood implemented in MEGA (Tamura *et al.*, 2011) (see Supporting Information Table S1 for details). To check for incongruence between the chloroplastic and nuclear datasets, we first analyzed both matrices separately using maximum likelihood with RAxML (v.8.0.20) and bayesian inference implemented in BEAST v.1.8.2 (Drummond & Rambaut, 2007) (Fig. S1). Finally, we combined the data to construct a time-calibrated phylogeny for the subfamily Callitroidae (Cupressaceae). We used the recognized position of *Papuacedrus* as sister to all other species in this group to root the tree (Leslie *et al.*, 2012; Mao *et al.*, 2012). We set a minimum constraint on the age of crown Callitroidae (Leslie *et al.*, 2012; Mao *et al.*, 2012) by using the Patagonian fossil *Papuacedrus prechilensis* (Wilf *et al.*, 2009), based on an ovulate cone from the early to mid-Eocene (51.9–47.5 Ma). The maximum age for the appearance of crown Callitroidae was conservatively set by evidence that crown Cupressaceae (i.e. subfamilies Callitroidae and Cupressoidae) was present by 99.6 Ma, using leafy shoots and cones of the fossil *Widdringtonia americana* from the Cenomanian (McIver, 2001). Although this fossil is probably too old to belong to the extant genus *Widdringtonia*, it definitely belongs to the Cupressaceae s.s., that is, excluding the Taxodioid lineages. We used the earliest evidence of *Callitris* (Paull & Hill, 2010) to constrain the crown of the *Callitris* clade. *C. leayana* from early Oligocene Tasmania has cone scales and leaves in whorls of three, which are easily distinguishable from *Fitzroya*, the only other extant genus with this arrangement. However, this fossil bears characters of both *Callitris* and *Actinostrobus*, and the phylogenetic relationships between the two genera are still ambiguous (Pye *et al.*, 2003; Piggin & Bruhl, 2010). Finally, we used *Fitzroya acutifolia* to calibrate the split between *Fitzroya* and *Diselma*, based on the high similarity between the fossil leaves and cones from the early Oligocene and extant *Fitzroya* (Paull & Hill, 2010). We used a uniform prior for the root calibration (49.9–99.6 Ma), and lognormal priors for the crown *Callitris* clade and the *Fitzroya–Diselma* split, specified so that the 95% confidence interval (CI) spanned 28.3–48.3 Ma. We ran the chain for 100 million generations, sampling every 10 000. We discarded the first 25% of the chain as burn-in and evaluated convergence using TRACER v.1.6 – all effective sample sizes were well above 200.

Statistical analyses

Vulnerability curve fitting was done in SAS 9.4 (SAS Institute Inc., Cary, NC, USA). All remaining data manipulation and analysis were run in R v.3.2.3 (R Core Team, 2015). We performed linear regressions on raw data and log-transformed data with nearly identical results, so we present only untransformed correlations to simplify interpretation. When significant relationships appeared nonlinear, we fitted a nonlinear model (i.e. $y = a \times \log(x) + b$) with nonlinear least-squares (NLS function) in

R. However, to allow comparisons across bivariate relationships, in all cases we report the R^2 values from the linear correlations. Phylogenetic generalized least squares (PGLS) were run using the CAPER package v.0.5.2 (Orme, 2013). PGLS accounts for the statistical nonindependence in cross-species trait correlations by adjusting the residual error structure using a variance/covariance matrix derived from the phylogeny (Garamszegi, 2014). It explicitly allows for varying amounts of phylogenetic signal in the data by using Pagel's lambda (Pagel, 1999), thus removing the risk of overcorrecting for phylogeny when shared evolutionary history does not affect trait relationships. We used PHYTOOLS v.0.5 (Revell, 2013) to map the evolution of P_{50} onto the time-calibrated phylogeny using a Brownian motion model of evolution and maximum likelihood. We used APE v.4.0 (Paradis *et al.*, 2004) to estimate ancestral states, to plot the number of lineages through time, and to obtain the gamma statistic (Pybus & Harvey, 2000).

Results

Variation in hydraulic traits

Xylem embolism resistance varied widely across the *Callitris* clade, from $P_{50} = -3.8 \pm 0.1$ MPa in *C. neocaledonica* to -18.8 ± 0.6 MPa in *C. tuberculata* (mean ± SE; Fig. 2; Table S2). P_{50} had a mean of -11.7 ± 0.7 MPa across the whole clade. Xylem specific hydraulic conductivity (K_s) varied approximately sixfold, from 0.187 ± 0.014 kg m^{-1} MPa^{-1} s^{-1} in *C. oblonga* to 1.25 ± 0.05 kg m^{-1} MPa^{-1} s^{-1} in *C. intratropica*, with a clade-wide mean of 0.52 ± 0.05 kg m^{-1} MPa^{-1} s^{-1}. Our analysis of xylem anatomy uncovered extensive variation, with some species containing many small, densely packed tracheids (e.g. *C. tuberculata*, mean diameter = 9.04 ± 0.23 µm, tracheid frequency = 3250 ± 126 n mm^{-2}), while others had fewer but wider tracheids (e.g. *C. sulcata*, 14.14 ± 0.77 µm and

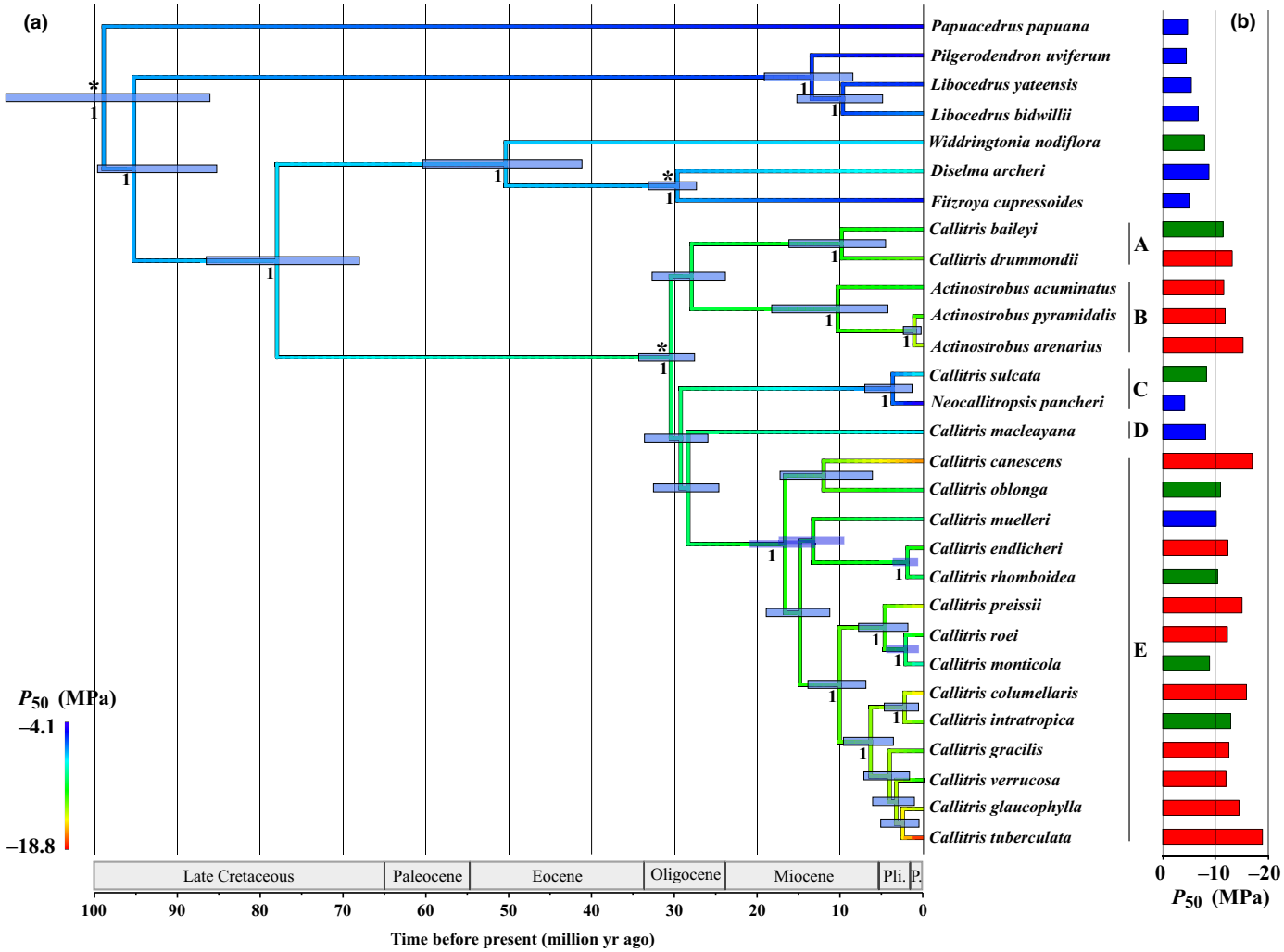

Fig. 2 Time-tree of Callitroidae and the evolution of resistance to embolism (P_{50}) in the *Callitris* clade. (a) Phylogeny of Callitroidae. Blue bars at nodes represent 95% highest posterior density from the BEAST analysis, and numbers represent Bayesian posterior probabilities (not shown if < 0.95). Branches of the phylogeny are colored according to P_{50} reconstructed using the Brownian motion model (scale bottom left). Stars mark fossil-calibrated nodes. Letters A–E indicate the five subclades within crown *Callitris*. (b) Bar plot of P_{50} for each species in the phylogeny, colored according to species aridity index (AI). Red, AI < 0.5; green, 0.5 < AI < 1; blue, AI > 1. *Callitris neocaledonica* is the only missing species: $P_{50} = -3.8$ MPa, AI = 2.0. Pli., Pliocene; P., Pleistocene.

1607 ± 178 n mm^{-2}). Accordingly, theoretical hydraulic conductance (K_{th}) also displayed a wide range of values, with the xylem of *C. sulcata* *c.* 10 times more efficient than that of *C. gracilis* (13.2 ± 1.7 and 1.15 ± 0.14 kg m^{-1} MPa^{-1} s^{-1}, respectively). Comparatively, variation in wood density was moderate yet significant, from 0.57 ± 0.02 g cm^{-3} in *C. oblonga* to a maximum of 0.74 ± 0.04 g cm^{-3} in *N. pancheri*.

Using occurrence data, we found that across the geographical range of the *Callitris* clade, mean annual precipitation (MAP) varied from *c.* 300 mm for *C. tuberculata* in Western Australia to over 2100 mm for *N. pancheri* in New Caledonia. Similar variation was found for the aridity index (AI), ranging from 0.21 to 2.03 for *C. tuberculata* and *C. neocaledonica*, respectively. Mean annual temperature varied from 12.8°C for *C. oblonga* to 26.8°C for *C. intratropica*.

We tested the role of water availability in determining species' hydraulic properties. More negative P_{50} was strongly related to increasing aridity across species ranges (Fig. 3a,b; $R^2 = 0.78$ and 0.81 for MAP and AI, respectively). This trend was confirmed using PGLS, proving the adaptive role of xylem embolism resistance in *Callitris*. There was nonetheless wide variation in P_{50} for similar rainfall values. For example, in the most arid environments with MAP < 450 mm, embolism resistance was in the range $P_{50} = -12$ to -19 MPa. Tracheid dimensions also track rainfall, with increasing precipitation associated with wider tracheids (Fig. 3g,h; $R^2 = 0.45$ and 0.48 for MAP and AI, respectively). Neither K_s (Fig. 3d–f) nor wood density (Fig. 3j–l) were linked to MAP in the studied clade. However, these traits were related to mean annual temperature, with warmer climates linked to higher transport efficiency and higher wood density, although R^2 values were low (Fig. 3f,l; $R^2 = 0.245$ and 0.135, respectively). By contrast, we found no evidence for an effect of temperature on P_{50} or tracheid diameter (Fig. 3c,i). Accounting for phylogenetic proximity using PGLS did not impact these trait–climate relationships (Table S3). We note that since MAP enters into the calculation of AI, these two variables are strongly correlated.

In our dataset, we found that P_{50} and tracheid diameter were strongly positively correlated, and P_{50} and tracheid frequency were negatively correlated, with resistant species having numerous smaller tracheids compared with species that were more vulnerable (Fig. 4a,b). No relationship was detected between P_{50} and void-to-wood ratio or wood density (Fig. 4c,d). In turn, K_s appeared to be disconnected to some extent from tracheid and wood traits, showing only a significant relationship with tracheid frequency (Fig. 4f). The remarkably high conductance measured for *C. intratropica* must be highlighted, as it is the result of a highly unusual combination of hydraulic traits: narrow D_h (Fig. 4e), low tracheid frequency (Fig. 4f), and moderate void-to-wood ratio (Fig. 4g) and wood density (Fig. 4h). Overall, hydraulic safety (P_{50}) and efficiency (K_s) were not closely linked to wood traits in the *Callitris* clade, yet resistant species developed smaller, more frequent tracheids. We also investigated the safety–efficiency tradeoff hypothesis, but we found no significant relationship between P_{50} and K_s (Fig. 5). In this line, bordered pit conductivity was unrelated to P_{50} (Fig. 5c). By contrast, theoretical maximum hydraulic conductance (K_{th}) was negatively correlated with xylem embolism resistance. Resistant species had a theoretically less efficient xylem when only considering tracheid lumen conductivity (Fig. 5b), which is consistent with smaller tracheids being related to embolism resistance (Fig. 4a). By contrast, bordered pit conductivity (K_{pit}) was unrelated to P_{50}, and remained around or below 1 kg m^{-1} MPa^{-1} s^{-1} across species (Fig. 5c). These relationships were not impacted by phylogenetic history (Table S4). Finally, tracheid length and average number of pits per tracheid were weakly correlated with embolism resistance, where more embolism-resistant species had shorter tracheids with fewer pits (e.g. *C. tuberculata*, 1167 ± 35 μm and 38 ± 2 pits) than more vulnerable species (e.g. *C. macleayana*, 1931 ± 43 μm and 81 ± 3 pits). However, higher pitting was not associated with an increase in overall conductance (Fig. S2).

Phylogeny and trait evolution

Our phylogenetic analyses recovered the well-recognized relationships within the subfamily Callitroidae, with the *Pilgerodendron–Libocedrus* clade sister to remaining species. The *Diselma-Fitzroya* clade is closely allied to *Widdringtonia* (Fig. 2). Within the *Callitris* s.l. group containing the paraphyletic *Callitris*, *Actinostrobus* and *Neocallitropsis*, early divergences dated to between 30 and 25 Ma are not well resolved (Fig. 2). We found five separate subclades (see letters in Fig. 2): *C. drummondii* and *C. baileyi* (A), the three *Actinostrobus* species (B), two tropical northeastern clades composed of the New Caledonian species *N. pancheri* and *C. sulcata* (B) and *C. macleayana* (C) and a well-supported core *Callitris* clade encompassing the remaining Australian species (E), which is comfortably the most species-rich group within *Callitris* (14 species).

When examining diversification trends, our phylogenetic analysis indicates an upward shift *c.* 30 Ma (Fig. 6a), with the rapid successive divergences of the five subclades identified in Fig. 2a. A second acceleration in diversification corresponds with the divergences in the core *Callitris* clade (clade E in Fig. 2a), *c.* 17 Ma and continuing to the present. Tempo of diversification varied through time, with a γ-statistic of 2.36 ($P = 0.02$), indicating either an early decrease in extinction rates or a pulse of speciation toward the present (Pybus & Harvey, 2000). By mapping the evolution of xylem embolism resistance onto the phylogeny, we showed that several lineages achieved extreme P_{50} under -15 MPa independently over the last 10 million yr, i.e. *A. arenarius*, *C. canescens*, *C. columellaris* and *C. tuberculata* (Fig. 2a). Overall, P_{50} was extremely labile, with large differences between closely related species, for example *C. monticola* and *C. roei* ($P_{50} = -8.8$ and -12.2 MPa, respectively), *C. oblonga* and *C. canescens* (-10.9 and -16.9 MPa), *N. pancheri* and *C. sulcata* (-4.1 and -8.2 MPa) and *A. pyramidalis* and *A. arenarius* (-11.8 and -15.2 MPa). Related species of the Callitroideae subfamily are relatively vulnerable to xylem embolism, e.g. *Papuacedrus papuana* ($P_{50} = -4.7$ MPa) and *Pilgerodendron uviferum* ($P_{50} = -4.4$ MPa). The ancestral P_{50} reconstruction inferred that the ancestral state in the Callitroidae subfamily was *c.* -7.2 MPa (95% CI: -1.6 to -12.4 MPa), and that the common ancestor of the *Callitris* clade was moderately resistant, with

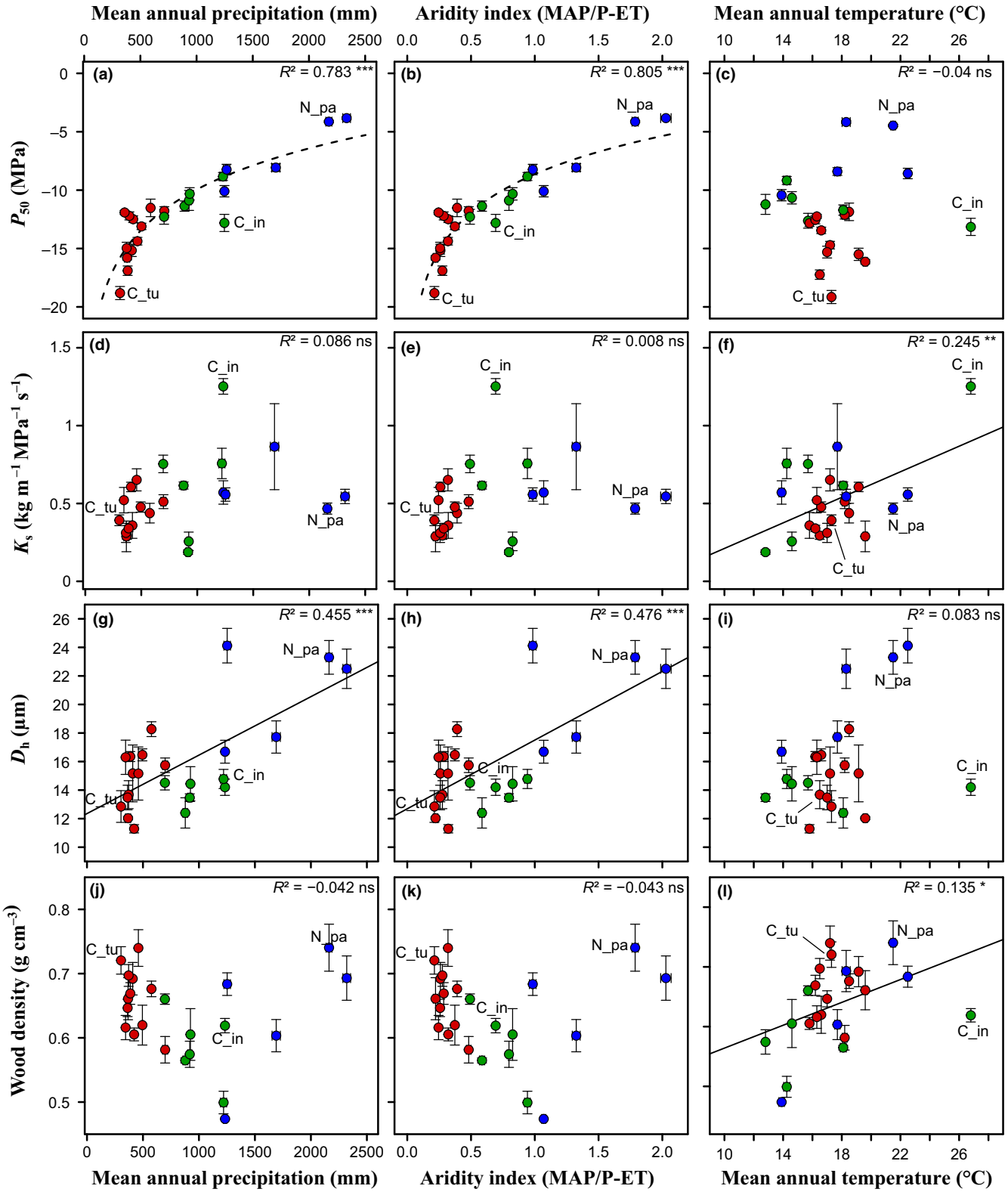

Fig. 3 Relationships between xylem hydraulic traits and climate in *Callitris*. (a–l) Embolism resistance (P_{50}; a–c), xylem specific hydraulic conductivity (K_s; d–f), hydraulically weighted tracheid diameter (D_h; g–i) and wood density (j–l) in relation to water availability, as measured by mean annual precipitation (MAP, left), aridity index (AI, centre) and mean annual temperature (right). Linear regression lines are shown, with the adjusted R^2. Statistical significance is indicated by asterisks: ***, $P < 0.001$; **, $P < 0.01$; *, $P < 0.05$; ns, nonsignificance at $\alpha = 0.05$. Dashed curves in (a) and (b) represent the best fit nonlinear model. C_tu, *Callitris tuberculate*; C_in, *C. intratropica*; N_pa, *Neocallitropsis pancheri*; P-ET, potential evapotranspiration. Red, AI < 0.5; green, 0.5 < AI < 1; blue, AI > 1. Error bars represent ± SE.

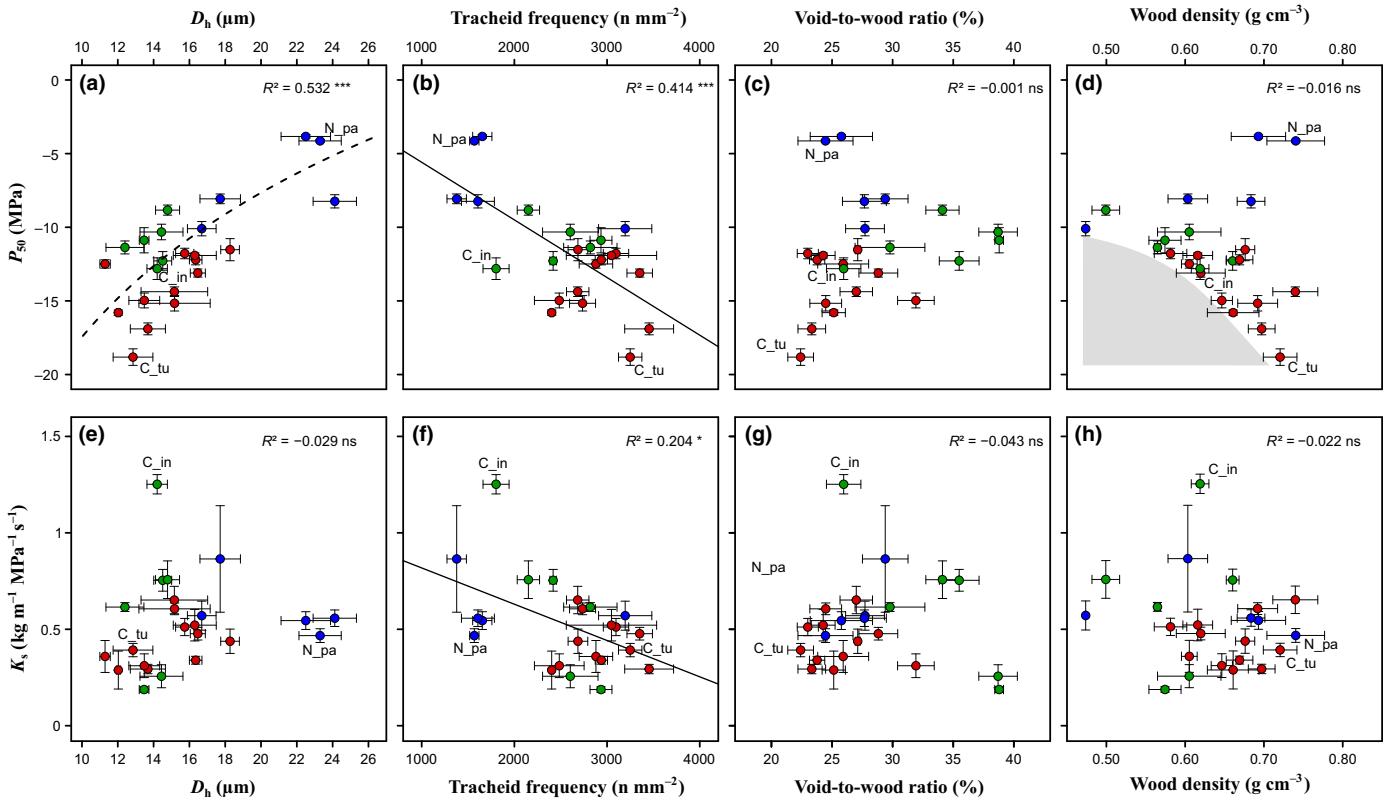

Fig. 4 Relationships between wood construction traits and hydraulic safety and efficiency in Callitris. Correlations between embolism resistance (P_{50}, upper panels) and xylem specific hydraulic conductivity (K_s, lower panels) and four wood traits: tracheid hydraulically weighted diameter (D_h) (a, e), tracheid frequency (b, f), void-to-wood ratio (c, g), and wood density (d, h). Linear regression lines are shown, with the adjusted R^2. Statistical significance is indicated by asterisks: ***, $P < 0.001$; *, $P < 0.05$; ns, nonsignificance at $\alpha = 0.05$. Error bars represent ± SE. The dotted line (a) is the best-fit nonlinear model. The shaded area in (d) shows trait space theoretically excluded owing to risk of tracheid implosion (Hacke et al., 2001). Red, aridity index (AI) < 0.5; green, 0.5 < AI < 1; blue, AI > 1. C_tu, *Callitris tuberculate*; C_in, *Callitris intratropica*; N_pa, *Neocallitropsis pancheri*.

P_{50} ~ −10.4 MPa (95% CI: −8 to −12.9 MPa). Details for the reconstructed P_{50} values at each node of the phylogeny can be found in Fig. S3.

Discussion

Evolution of P_{50} and the adaptive radiation of *Callitris*

Our results provide strong evidence that the evolution of extreme xylem embolism resistance accompanied the radiation of the *Callitris* clade and was driven by the aridification of the Australian continent during the last 30 million yr.

The *Callitris* clade is by far the most embolism-resistant group of trees in the world, containing multiple extreme P_{50} records (i.e. *C. glaucophylla* (−14.4 MPa), *C. preissii* (−15 MPa), *A. arenarius* (−15.2 MPa), *C. columellaris* (−15.8 MPa), *C. canescens* −16.9 MPa) and *C. tuberculata* (−18.8 MPa)). Only a handful of other gymnosperm species reach P_{50} values lower than −13 MPa, for example in *Juniperus* (Willson *et al.*, 2008; Choat *et al.*, 2012) and *Tetraclinis* (Bouche *et al.*, 2014), and also conifers from the Cupressaceae family. Previous studies at broader evolutionary and geographical scales found a weak P_{50}–rainfall relationship, reporting both vulnerable and resistant species in areas of low precipitation (Brodribb & Hill, 1999; Maherali *et al.*, 2004; Choat *et al.*, 2012; Brodribb *et al.*, 2014). By contrast, our study at a regional, more restricted evolutionary scale reveals a strong relation between xylem embolism resistance and MAP (Fig. 2a). Further, our results suggest that variation in P_{50} can be largely predicted by local AI (Fig. 2b). These results reveal two contrasting patterns in extant *Callitris* that either occupy high rainfall environments and have relatively vulnerable xylem or are distributed in xeric or seasonally dry environments with much less vulnerable xylem.

The poor fossil record of *Callitris* (Hill & Brodribb, 1999; Paull & Hill, 2010) and uncertainty in deep divergences in both our study and previous work (Pye *et al.*, 2003; Piggin & Bruhl, 2010) shrouds in uncertainty the inference of ancestral ecology or drought tolerance in the *Callitris* clade. However, our mapping of P_{50} across the Callitroidae suggests that the vascular apparatus of the last common ancestor of *Callitris* was less resistant to drought-induced xylem embolism (Fig. 2a). In line with our results, the earliest definite fossil member of this clade is dated to *c.* 30 Ma and is associated with an assemblage of rainforest taxa, but shares characters with modern *Callitris* species found in both dry and wet environments (Paull & Hill, 2010). Before this time most of Australia was covered with warm and temperate rainforests, with year-round wet climates, but the end of the Eocene (34 Ma) is marked by a global cooling event and a major drop in

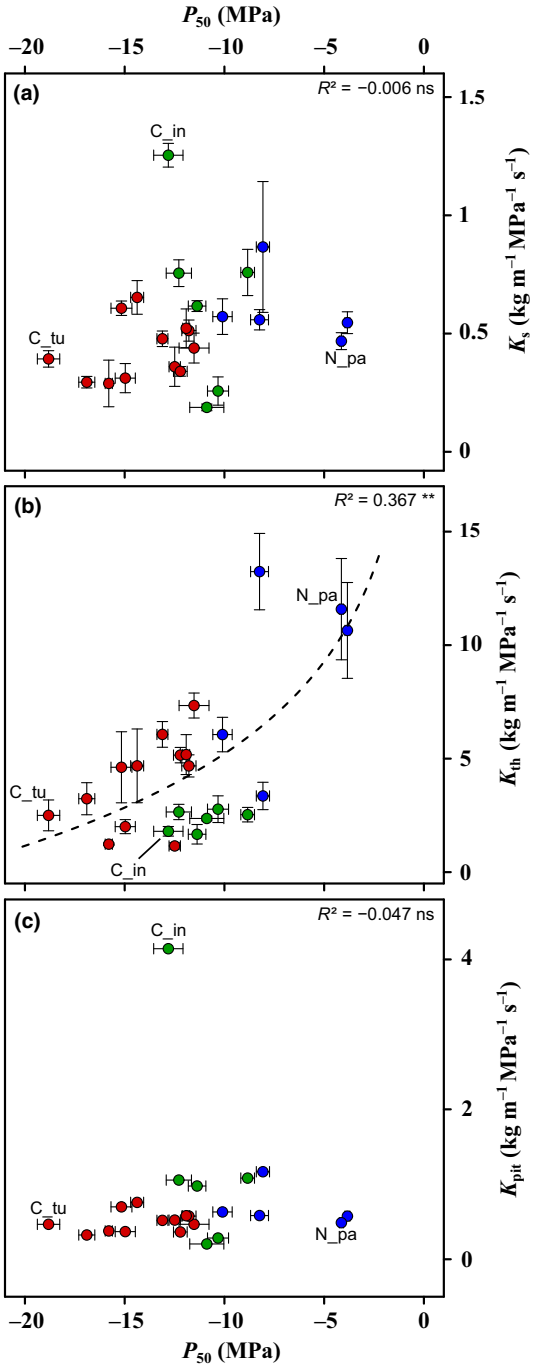

Fig. 5 Xylem safety vs efficiency relationship in *Callitris*. (a–c) Embolism resistance (P_{50}) in relation to xylem specific hydraulic conductivity (K_s; a), theoretical conductance (K_{th}; b), and the derived total pit conductivity (K_{pit}; c). Linear regressions are reported with R^2. Statistical significance is indicated by asterisks: **, $P < 0.01$; ns, nonsignificance at $\alpha = 0.05$. The dashed line (b) is the best-fit nonlinear model. Red, aridity index (AI) < 0.5; green, 0.5 < AI < 1; blue, AI > 1. C_tu, *Callitris tuberculate*; C_in, *C. intratropica*; N_pa, *Neocallitropsis pancheri*.

sea level (Martin, 2006; Macphail, 2007). This cooling trend is visible in the oxygen-isotope composition record (Fig. 6c) and is linked to lower rainfall based on paleosols from central Australia (Fig. 6b). Concomitantly, vegetation shifts indicate the existence of dry seasons and the emergence of the open woodland ecosystems, at least in central Australia (Crisp *et al.*, 2004; Martin, 2006; Fujioka & Chappell, 2010). The onset of more severe aridity in mainland Australia is dated to the mid-Miocene (Martin, 2006; Fujioka & Chappell, 2010; Metzger & Retallack, 2010). The extreme aridity over much of central Australia today is relatively young and linked to the glacial cycles in the northern hemisphere *c.* 1–4 Ma; (Crisp *et al.*, 2004; Byrne *et al.*, 2008). Over this period, highly resistant xylem seems to have evolved multiple times independently in different lineages within the group, as a result of convergent evolution. For instance, analogous low P_{50} values are expressed in *Actinostrobus* and in the rest of the *Callitris* clade. Meanwhile, our analysis found that the diversification of the *Callitris* clade happened in two successive pulses, the first at *c.* 30 Ma and the second from the mid-Miocene onwards (i.e. from *c.* 16 Ma to the present), coinciding with the major shifts in the climate of the region. This may underpin increasing aridification as a major driving force in *Callitris* evolutionary history, and the evolution of extreme xylem embolism resistance as a main trigger of their diversification, providing *Callitris* with an outstanding competitive advantage over the last 30 million yr.

On the lower end of the *Callitris* xylem embolism resistance spectrum, we find a group of New Caledonian species (clade C; Fig 2a), which occur in tropical forests with significantly higher rainfall regimes. Previous work has shown that past climatic refugia may have persisted in the New Caledonia during the last glacial cycle, mitigating the significant drought that affected the region (Pouteau *et al.*, 2015). The high P_{50} values observed in the New Caledonian clade may therefore result from a lack of drought-exerted selective pressure. Despite the remarkable diversity of conifers in New Caledonia (Jaffré *et al.*, 1994; De Laubenfels, 1996), the *Callitris* clade is poorly represented with only three species, compared with 13 species of *Araucaria*. These are highly vulnerable to xylem embolism, with P_{50} typically in the range of −2 to −3 MPa (Bouche *et al.*, 2014; Zimmer *et al.*, 2016). Both these groups are threatened by climate change, as a result of their fragmented distributions and reduced habitat linked to human activity (Beaumont *et al.*, 2011; Pouteau & Birnbaum, 2016). These taxa have different histories in Australia: *Araucaria* diversity has declined to only two extant species over the last 30 million yr (Kershaw & Wagstaff, 2001), probably because of their limited tolerance to drought (Zimmer *et al.*, 2016). On the other hand, *Callitris* has thrived, largely thanks to the evolution of its xylem driven by reduced water availability.

Coevolution of xylem traits

A drought tolerance strategy based on a highly embolism-resistant xylem is expected to come with costs, notably with higher carbon investment in conduit walls to cope with extreme xylem tensions and a reduction in water transport efficiency as a result of the associated reduction in conduit size (Hacke *et al.*, 2001; Sperry, 2003; Pittermann *et al.*, 2006a,b, 2011). High embolism resistance in xeric *Callitris* species is associated with small conduits, which is consistent with the trend in conifers and angiosperms (Sperry *et al.*, 2006). Similarly to the trend across all

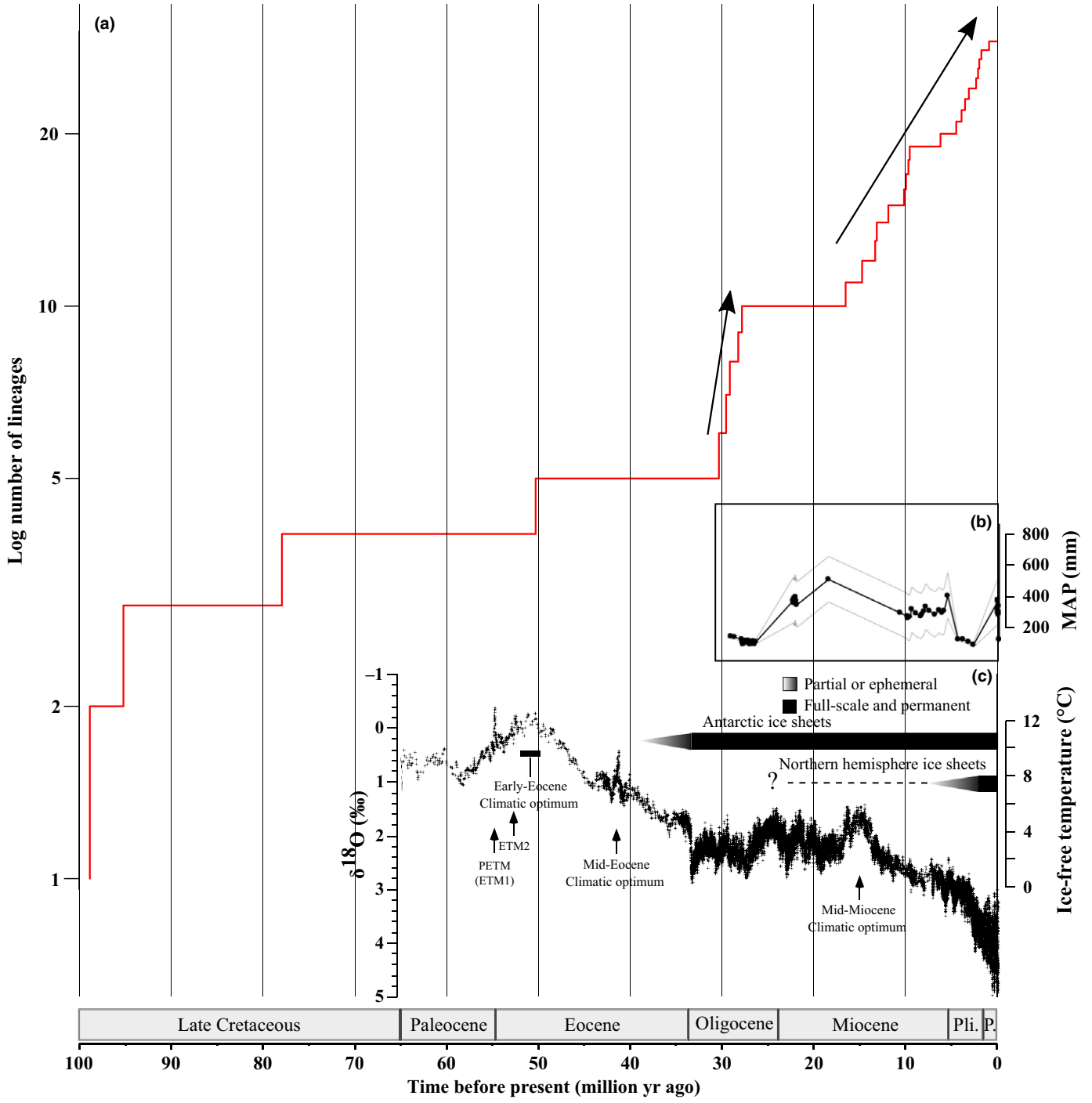

Fig. 6 Diversification of *Callitris* and climate trends of the past 65 million yr. (a) Lineage through time plot on log-scale. Two periods of higher diversification rate are indicated by black arrows. (b) Estimated mean annual precipitation (MAP; mm yr^{-1}) in Central Australia for the last 30 million yr, based on paleosol analysis (Metzger & Retallack, 2010). (c) Global temperature trend for the last 65 million yr. Data is deep-sea benthic foraminiferal oxygen isotopic composition ($\delta^{18}O$; ‰, left axis), a proxy for global temperature (Zachos *et al.*, 2001, 2008). The temperature scale (right axis) indicates the corresponding temperature, but is only valid for an ice-free world (i.e. not for periods with extensive ice at the poles (from *c.* 35 Ma)). Pli., Pliocene; P., Pleistocene. PETM, Paleocene-Eocene Thermal Maximum; ETM1-2, Eocene Thermal Maximum 1-2.

conifers (Hacke *et al.*, 2001), we found no species with high embolism resistance and low wood density. However, we found no evidence of an influence of aridity or P_{50} on wood density, and the highest wood density was found in *N. pancheri*, the species with the highest P_{50} measured in this study, a small slow-growing tree found on ultramafic soils in hot tropical climates with high rainfall. Wood density is a key functional trait that is determined by many factors, for example ring width, temperature and soil fertility (Chave *et al.*, 2006; Heineman *et al.*, 2016). It is worth noting here that all three New Caledonian species have high wood density and are found on skeletal, poor ultramafic soils, characterized by low concentrations of nitrogen, potassium,

phosphorus, and calcium, and sometimes toxic concentrations of magnesium, nickel and manganese (Jaffré, 1995). Additionally, and in spite of a significant reduction in tracheid diameter, we found no significant decrease in xylem specific hydraulic conductance with increasing aridity and increasing resistance to embolism. This is in agreement with the lack of a linear trend across all conifers (Brodribb & Hill, 1999; Gleason *et al.*, 2016).

How do embolism-resistant *Callitris* species maintain high water flow while reducing tracheid diameter? Xylem specific conductivity in conifers is strongly influenced by tracheid length and the total area of pits connecting adjacent tracheids (Pittermann *et al.*, 2005). In *Callitris*, however, we found no evidence of a relationship between tracheid length or number of pits and K_s, while more resistant species did tend to have shorter tracheids and fewer pits (Fig. S2). This could be linked to the increased probability of a rare 'leaky' pit in tracheids with more numerous pits, similar to the 'rare pit' hypothesis in angiosperms (Choat *et al.*, 2003; Wheeler *et al.*, 2005). Resistance of pits to water flow is mainly linked to the size and distribution of pores in the pit membrane and the depth and width of the pit aperture tunnel (Hacke *et al.*, 2004; Bouche, 2015). Embolism resistance is linked to the sealing of the pit aperture by the torus in conifers (Domec *et al.*, 2006; Cochard *et al.*, 2009; Delzon *et al.*, 2010; Pittermann *et al.*, 2010; Bouche *et al.*, 2014). Increasing torus size relative to pit aperture (i.e. increasing torus overlap) has been shown to be related to more negative P_{50}, but does not reduce overall pit conductivity, which is mostly related to the size of pores in the margo and the pit aperture dimensions (Hacke *et al.*, 2004; Pittermann *et al.*, 2010; Bouche, 2015). Our results demonstrate that in the *Callitris* clade, water flow through vascular tissue is mostly limited by pit resistivity, indicated by $K_{pit} << K_{th}$, as in other conifers (Pittermann *et al.*, 2006a). Additionally, bordered pits can be efficient for water transport, leading to high values of K_{pit}, and can also limit air-seeding under high xylem tension (Pittermann *et al.*, 2005; Domec *et al.*, 2006). A prime example is *C. intratropica*, with average tracheid diameters ($D_h = 14.2$ µm; see Fig. 3) but by far the highest xylem conductivity in *Callitris* ($125\ 10^{-5}$ m² MPa^{-1} s^{-1}), coupled with highly resistant xylem ($P_{50} = -12.8$ MPa).

In other conifer genera, variation in xylem embolism resistance seems to be limited, for example in *Pinus*, in which P_{50} varies between *c.* −3 and −5 MPa (Delzon *et al.*, 2010). The extraordinary lability of embolism resistance in the *Callitris* clade is probably linked to their capacity to uncouple xylem safety from construction cost and xylem efficiency. Additionally, *Callitris* species display a typical anisohydric behavior, allowing the xylem midday water potential to track declining soil water potential during drought (Brodribb *et al.*, 2013). Unlike many other conifer species, they use leaf desiccation rather than high concentrations of ABA to induce stomatal closure, allowing them to recover more quickly after rewatering (Brodribb & McAdam, 2013; Brodribb *et al.*, 2014). However, continued leakage of water vapor from the leaf surface through closed stomata exposes their xylem to more negative water potential during prolonged drought – hence the need for more negative P_{50} to avoid embolism-induced loss of hydraulic conductance. This derived strategy is followed by both *Callitris* and their sister-taxa in the Callitroidae subfamily (e.g. *Austrocedrus*, *Widdringtonia*, *Fitzroya*). A possible cost of this strategy could be the reinforcement of the leaves of these species, allowing them to endure extremely low leaf water potential before suffering leaf damage during drought (e.g. −8 MPa in *Callitris rhomboidea* (Brodribb *et al.*, 2014), and −11 MPa in *C. columellaris* and *C. preissii* (Brodribb *et al.*, 2010)). The more conservative water management strategy evident in many other conifers (e.g. Pinaceae, Araucariaceae) could help to explain the absence of very high embolism resistance in these clades (Delzon *et al.*, 2010; Brodribb *et al.*, 2014).

Our results confirm the evolutionary lability of xylem resistance to embolism, with a transition towards extreme resistance of several species within the *Callitris* clade. Combined with the onset of severe aridity in Australia, our results detail the remarkable adaptive radiation of this group. Despite overwhelming evidence for the role of decreasing water availability in shaping xylem traits, we found no evidence of its effect on xylem water transport efficiency and wood density. Species from more xeric areas develop smaller tracheids, but both wood traits and embolism resistance are totally disconnected from overall xylem conductivity. This suggests a lack of tradeoffs between construction costs and safety, on the one hand, and efficiency on the other. We also highlight a likely evolutionary role of pit-level traits in this clade, regarding hydraulic safety and efficiency. While this clade has shown a remarkable capacity to adapt and even thrive in increasingly arid conditions, modern climate change largely exceeds the pace of past climate upheavals. Many of the more vulnerable *Callitris* species have small restricted distributions and are already threatened by habitat destruction through land-use change and regular fires (IUCN, 2015), and could therefore be in severe danger of extinction in the coming decades.

Acknowledgements

The authors acknowledge Lin Kozlowski and Renee Smith for their analyses of wood anatomical traits, Anita Wesolowski and Vanessa Hequet for help with conducting sampling for this study, Frédéric Lagane for assistance with the wood density measurements, and Gaelle Capdeville for assistance with embolism assessment. The authors thank Stacey Smith for helpful comments on a previous version of the manuscript, and three anonymous reviewers for their suggestions to improve the manuscript. Part of this study was funded by the programme 'Investments for the Future' (grant no. ANR-10-EQPX-16, XYLOFOREST) from the French National Agency for research, and mobility grants within the COTE Cluster of Excellence (grant no. ANR-10-LABX-45).

Author contributions

M.L., S.P., J-C.D. and S.D. designed the research; M.L., S.P., S.T. and S.D. collected the samples; N.N. provided DNA sequences; M.L. and S.P. measured the hydraulic traits; M.L. analyzed the data, ran the phylogenetic analysis, and led the manuscript preparation. All authors contributed to the writing of the manuscript.

References

Anderegg WRL, Berry JA, Smith DD, Sperry JS, Anderegg LDL, Field CB. 2012. The roles of hydraulic and carbon stress in a widespread climate-induced forest die-off. *Proceedings of the National Academy of Sciences, USA* **109**: 233–237.

Anderegg WRL, Klein T, Bartlett M, Sack L, Pellegrini AFA, Choat B. 2016. Meta-analysis reveals that hydraulic traits explain cross-species patterns of drought-induced tree mortality across the globe. *Proceedings of the National Academy of Sciences, USA* **113**: 2–7.

Antonelli AE, Verola CF, Parisod CN, Gustafsson ALS. 2010. Climate cooling promoted the expansion and radiation of a threatened group of South American orchids (Epidendroideae: Laeliinae). *Biological Journal of the Linnean Society* **100**: 597–607.

Augusto L, Davies TJ, Delzon S, De Schrijver A. 2014. The enigma of the rise of angiosperms: can we untie the knot? *Ecology Letters* **17**: 1326–1338.

Bailey IW. 1916. The structure of the bordered pits of conifers and its bearing upon the tension hypothesis of the ascent of sap in plants. *Botanical Gazette* **62**: 133.

Beaumont LJ, Pitman A, Perkins S, Zimmermann NE, Yoccoz NG. 2011. Impacts of climate change on the world's most exceptional ecoregions. *Proceedings of the National Academy of Sciences, USA* **108**: 2306–2311.

Benson DA, Karsch-Mizrachi I, Lipman DJ, Ostell J, Sayers EW. 2011. GenBank. *Nucleic Acids Research* **39**: D32–D37.

Booth TH. 2014. Using biodiversity databases to verify and improve descriptions of tree species climatic requirements. *Forest Ecology and Management* **315**: 95–102.

Bouche PS. 2015. Cavitation resistance and the functional role of bordered pits in xylem of conifers – from inter-specific to within tree variability. Unpublished doctoral thesis, Universität Ulm, Germany.

Bouche PS, Jansen S, Sabalera JC, Cochard H, Burlett R, Delzon S. 2016. Low intra-tree variability in resistance to embolism in four Pinaceae species. *Annals of Forest Science* **73**: 681–689.

Bouche PS, Larter M, Domec J-C, Burlett R, Gasson P, Jansen S, Delzon S. 2014. A broad survey of hydraulic and mechanical safety in the xylem of conifers. *Journal of Experimental Botany* **65**: 4419–4431.

Bowman DMJS, Prior LD, Tng DYP, Hua Q, Brodribb TJ. 2011. Continental-scale climatic drivers of growth ring variability in an Australian conifer. *Trees* **25**: 925–934.

Brodribb TJ, Bowman DMJS, Grierson PF, Murphy BP, Nichols S, Prior LD. 2013. Conservative water management in the widespread conifer genus *Callitris*. *AoB Plants* **5**: 1–11.

Brodribb TJ, Bowman DJMS, Nichols S, Delzon S, Burlett R. 2010. Xylem function and growth rate interact to determine recovery rates after exposure to extreme water deficit. *New Phytologist* **188**: 533–542.

Brodribb TJ, Cochard H. 2009. Hydraulic failure defines the recovery and point of death in water-stressed conifers. *Plant Physiology* **149**: 575–584.

Brodribb T, Hill RS. 1999. The importance of xylem constraints in the distribution of conifer species. *New Phytologist* **143**: 365–372.

Brodribb TJ, McAdam SAM. 2013. Abscisic acid mediates a divergence in the drought response of two conifers. *Plant Physiology* **162**: 1370–1377.

Brodribb TJ, McAdam SAM, Jordan GJ, Martins SCV. 2014. Conifer species adapt to low-rainfall climates by following one of two divergent pathways. *Proceedings of the National Academy of Sciences, USA* **111**: 14489–14493.

Byrne M, Yeates DK, Joseph L, Kearney M, Bowler J, Williams MAJ, Cooper S, Donnellan SC, Keogh JS, Leys R *et al.* 2008. Birth of a biome: insights into the assembly and maintenance of the Australian arid zone biota. *Molecular Ecology* **17**: 4398–4417.

Carpenter RJ, Hill RS, Jordan GJ. 1994. Cenozoic vegetation in Tasmania: macrofossil evidence. In: Hill RS, ed. *History of the Australian vegetation: cretaceous to recent*. Cambridge, UK: Cambridge University Press, 276.

Chave J, Muller-Landau HC, Baker TR, Easdale TA, ter Steege H, Webb CO. 2006. Regional and phylogenetic variation of wood density across 2456 Neotropical tree species. *Ecological Applications: A Publication of the Ecological Society of America* **16**: 2356–2367.

Choat B, Ball M, Luly J, Holtum J. 2003. Pit membrane porosity and water stress-induced cavitation in four co-existing dry rainforest tree species. *Plant Physiology* **131**: 41–48.

Choat B, Cobb AR, Jansen S. 2008. Structure and function of bordered pits: new discoveries and impacts on whole-plant hydraulic function. *New Phytologist* **177**: 608–626.

Choat B, Jansen S, Brodribb TJ, Cochard H, Delzon S, Bhaskar R, Bucci SJ, Feild TS, Gleason SM, Hacke UG *et al.* 2012. Global convergence in the vulnerability of forests to drought. *Nature* **491**: 752–755.

Cochard H, Damour G, Bodet C, Tharwat I, Poirier M, Améglio T. 2005. Evaluation of a new centrifuge technique for rapid generation of xylem vulnerability curves. *Physiologia Plantarum* **124**: 410–418.

Cochard H, Hölttä T, Herbette S, Delzon S, Mencuccini M. 2009. New insights into the mechanisms of water-stress-induced cavitation in conifers. *Plant Physiology* **151**: 949–954.

Corlett RT, Westcott DA. 2013. Will plant movements keep up with climate change? *Trends in Ecology & Evolution* **28**: 482–488.

Crisp M, Cook L, Steane D. 2004. Radiation of the Australian flora: what can comparisons of molecular phylogenies across multiple taxa tell us about the evolution of diversity in present-day communities? *Philosophical Transactions of the Royal Society of London. Series B, Biological Sciences* **359**: 1551–1571.

Crisp MD, Cook LG. 2011. Cenozoic extinctions account for the low diversity of extant gymnosperms compared with angiosperms. *New Phytologist* **192**: 997–1009.

David-Schwartz R, Paudel I, Mizrachi M, Shklar G, Delzon S, Cochard H, Lukyanov V, Badel E, Capdeville G, Cohen S. 2016. Evidence for genetic differentiation in vulnerability to embolism in Pinus halepensis. *Frontiers in Plant Science* **7**: 1–13.

Davis MB, Shaw RG. 2001. Range shifts and adaptive responses to Quaternary climate change. *Science* **292**: 673–680.

De Laubenfels DJ. 1996. Gondwanan conifers on the Pacific Rim. In: Keast A, Miller S, eds. *The origin and evolution of Pacific Island biotas, New Guinea to Eastern Polynesia: patterns and processes*. Amsterdam, the Netherlands: SPB Academic Publishing, 261–265.

Delzon S, Cochard H. 2014. Recent advances in tree hydraulics highlight the ecological significance of the hydraulic safety margin. *New Phytologist* **203**: 355–358.

Delzon S, Douthe C, Sala A, Cochard H. 2010. Mechanism of water-stress induced cavitation in conifers: bordered pit structure and function support the hypothesis of seal capillary-seeding. *Plant, Cell and Environment* **33**: 2101–2111.

Dixon HH. 1914. *Transpiration and the ascent of sap in plants*. London, UK: MacMillan.

Domec J-C, Lachenbruch B, Meinzer FC. 2006. Bordered pit structure and function determine spatial patterns of air-seeding thresholds in xylem of douglas-fir (*Pseudotsuga menziesii*; Pinaceae) trees. *American Journal of Botany* **93**: 1588–1600.

Drummond AJ, Rambaut A. 2007. BEAST: Bayesian evolutionary analysis by sampling trees. *BMC Evolutionary Biology* **7**: 214.

Dupont LM, Linder HP, Rommerskirchen F, Schefuß E. 2011. Climate-driven rampant speciation of the Cape flora. *Journal of Biogeography* **38**: 1059–1068.

Eckenwalder JE. 2009. *Conifers of the world: the complete reference*. Portland OR, USA and London, UK: Timber Press.

Eiserhardt WL, Borchsenius F, Plum CM, Ordonez A, Svenning JC. 2015. Climate-driven extinctions shape the phylogenetic structure of temperate tree floras. *Ecology Letters* **18**: 263–272.

Farjon A. 2005. *A monograph of Cupressaceae and Sciadopitys*. Kew, UK: Royal Botanic Gardens, Kew.

Farjon A. 2010. *A handbook of the world's conifers (2 Vols.)*. Leiden, the Netherlands: BRILL.

Franklin GL. 1945. Preparation of thin sections of synthetic resins and woody resin composites and a new method for wood. *Nature* **155**: 3924–3951.

Fujioka T, Chappell J. 2010. History of Australian aridity: chronology in the evolution of arid landscapes. *Geological Society Special Publication* **346**: 121–139.

Garamszegi Z. 2014. *Modern phylogenetic comparative methods and their application in evolutionary biology*. London, UK: Springer.

Gleason SM, Westoby M, Jansen S, Choat B, Hacke UG, Pratt RB, Bhaskar R, Brodribb TJ, Bucci SJ, Mayr S *et al.* 2016. Weak tradeoff between xylem safety and xylem-specific hydraulic efficiency across the world's woody plant species. *New Phytologist* **209**: 123–136.

Guay R, Gagnon R, Morin H. 1992. A new automatic and interactive tree ring measurement system based on a line scan camera. *The Forestry Chronicle* **68**: 138–141.

Hacke UG, Sperry JS, Pittermann J. 2004. Analysis of circular bordered pit function II. Gymnosperm tracheids with torus-margo pit membranes. *American Journal of Botany* **91**: 386–400.

Hacke UG, Sperry JS, Pittermann J. 2005. Efficiency versus safety tradeoffs for water conduction in angiosperm vessels versus gymnosperm tracheids. In: Holbrook MN, Zwieniecki MA, eds. *Vascular transport in plants*. Burlington, VT, USA: Elsevier Academic Press, 333–353.

Hacke UG, Sperry JS, Pockman WT, Davis SD, McCulloh KA. 2001. Trends in wood density and structure are linked to prevention of xylem implosion by negative pressure. *Oecologia* **126**: 457–461.

Hacke UG, Sperry JS, Wheeler JK, Castro L. 2006. Scaling of angiosperm xylem structure with safety and efficiency. *Tree Physiology* **26**: 689–701.

Hajek P, Kurjak D, von Wühlish G, Delzon S, Schuldt B. 2016. Intraspecific variation in wood anatomical, hydraulic and foliar traits in ten European beech provenances differing in growth yield. *Frontiers in Plant Science* **7**: 791.

Heineman KD, Turner BL, Dalling JW. 2016. Variation in wood nutrients along a tropical soil fertility gradient. *New Phytologist* **211**: 440–454.

Hijmans RJ, Cameron SE, Parra JL, Jones PG, Jarvis A. 2005. Very high resolution interpolated climate surfaces for global land areas. *International Journal of Climatology* **25**: 1965–1978.

Hill KD. 1998. Introduction to the Gymnosperms; Coniferophyta; Cycadophyta; Pinophyta. In: Orchard AE, ed. *Flora of Australia vol. 48, Ferns, gymnosperms, and allied groups*. Canberra, ACT, Australia: CSIRO, 581–587.

Hill RS. 2004. Origins of the southeastern Australian vegetation. *Philosophical Transactions of the Royal Society of London. Series B: Biological Sciences* **359**: 1537–1549.

Hill RS, Brodribb TJ. 1999. Southern conifers in time and space. *Australian Journal of Botany* **47**: 639–696.

Hua X, Wiens JJ. 2013. How does climate influence speciation? *The American Naturalist* **182**: 1–12.

IUCN. 2015. The IUCN red list of threatened species. Version 2015-4. [WWW document] URL http://www.iucnredlist.org/ [accessed 28 February 2017].

Jaffré T. 1995. Distribution and ecology of the conifers of New Caledonia. In: Enright NJ, Hill RS, eds. *Ecology of the southern conifers*. Melbourne, Vic., Australia: Melbourne University Press, 171–196.

Jaffré T, Morat P, Veillon JM. 1994. Dossier Nouvelle Calédonie: Caractéristiques et composition floristique des principales formations végétales. *Bois et Forêts des Tropiques* **242**: 7–30.

Kershaw P, Wagstaff B. 2001. The Southern Conifer family Araucariaceae: history, status, and value for paleoenvironmental reconstruction. *Annual Review of Ecology and Systematics* **32**: 397–414.

Koenen EJM, Clarkson JJ, Pennington TD, Chatrou LW. 2015. Recently evolved diversity and convergent radiations of rainforest mahoganies (Meliaceae) shed new light on the origins of rainforest hyperdiversity. *New Phytologist* **207**: 327–339.

Lamy J-B, Bouffier L, Burlett R, Plomion C, Cochard H, Delzon S. 2011. Uniform selection as a primary force reducing population genetic differentiation of cavitation resistance across a species range. *PLoS ONE* **6**: e23476.

Larter M, Brodribb TJ, Pfautsch S, Burlett R, Cochard H, Delzon S. 2015. Extreme aridity pushes trees to their physical limits. *Plant Physiology* **168**: 804–807.

Lens F, Tixier A, Cochard H, Sperry JS, Jansen S, Herbette S. 2013. Embolism resistance as a key mechanism to understand adaptive plant strategies. *Current Opinion in Plant Biology* **16**: 287–292.

Leslie AB, Beaulieu JM, Rai HS, Crane PR, Donoghue MJ, Mathews S. 2012. Hemisphere-scale differences in conifer evolutionary dynamics. *Proceedings of the National Academy of Sciences, USA* **109**: 16217–16221.

Li S, Lens F, Espino S, Karimi Z, Klepsch M, Schenk HJ, Schmitt M, Schuldt B, Jansen S. 2016. Intervessel pit membrane thickness as a key determinant of embolism resistance in angiosperm xylem. *IAWA Journal* **37**: 152–171.

Lübbe T, Schuldt B, Leuschner C. 2016. Acclimation of leaf water status and stem hydraulics to drought and tree neighbourhood: alternative strategies among the saplings of five temperate deciduous tree species. *Tree Physiology*: 1–13, doi.org/10.1093/treephys/tpw095.

Macphail M. 2007. *Australian palaeoclimates: Cretaceous to Tertiary: a review of palaeobotanical and related evidence to the year 2000*. CRC LEME Special Volume Open File Report 151. Bentley, WA: CSIRO, 1–266.

Maherali H, Pockman WT, Jackson RB. 2004. Adaptive variation in the vulnerability of woody plants to xylem cavitation. *Ecology* **85**: 2184–2199.

Mao K, Milne RI, Zhang L, Peng Y, Liu J, Thomas P, Mill RR, Renner SS. 2012. Distribution of living Cupressaceae reflects the breakup of Pangea. *Proceedings of the National Academy of Sciences, USA* **109**: 7793–7798.

Martin HA. 2006. Cenozoic climatic change and the development of the arid vegetation in Australia. *Journal of Arid Environments* **66**: 533–563.

McIver AEE. 2001. Cretaceous *Widdringtonia* Endl. (Cupressaceae) from North America. *International Journal of Plant Sciences* **162**: 937–961.

Metzger CA, Retallack GJ. 2010. Paleosol record of Neogene climate change in the Australian outback. *Australian Journal of Earth Sciences* **57**: 871–885.

Meyers LA, Bull JJ. 2002. Fighting change with change: adaptive variation in an uncertain world. *Trends in Ecology & Evolution* **17**: 551–557.

Mittelbach GG, Schemske DW, Cornell HV, Allen AP, Brown JM, Bush MB, Harrison SP, Hurlbert AH, Knowlton N, Lessios HA *et al.* 2007. Evolution and the latitudinal diversity gradient: speciation, extinction and biogeography. *Ecology Letters* **10**: 315–331.

Olson DM, Dinerstein E, Wikramanayake ED, Burgess ND, Powell GVN, Underwood EC, D'amico JA, Itoua I, Strand HE, Morrison JC *et al.* 2001. Terrestrial ecoregions of the world: a new map of life on Earth. *BioScience* **51**: 933–938.

Orme D. 2013. *The caper package : comparative analysis of phylogenetics and evolution in R. R package version 0.5, 2: 1–36.* [WWW document] URL https://cran.r-project.org/web/packages/caper/vignettes/caper.pdf [accessed 28 February 2017].

Pagel M. 1999. Inferring the historical patterns of biological evolution. *Nature* **401**: 877–884.

Pammenter NW, Vander Willigen C. 1998. A mathematical and statistical analysis of the curves illustrating vulnerability of xylem to cavitation. *Tree Physiology* **18**: 589–593.

Paradis E, Claude J, Strimmer K. 2004. APE: analyses of phylogenetics and evolution in R language. *Bioinformatics* **20**: 289–290.

Paull R, Hill RS. 2010. Early Oligocene *Callitris* and *Fitzroya* (Cupressaceae) from Tasmania. *American Journal of Botany* **97**: 809–820.

Pennington RT, Lavin M, Prado DE, Pendry CA, Pell SK, Butterworth CA. 2004. Historical climate change and speciation: neotropical seasonally dry forest plants show patterns of both Tertiary and Quaternary diversification. *Philosophical Transactions of the Royal Society of London. Series B, Biological Sciences* **359**: 515–537.

Pfautsch S. 2016. Hydraulic anatomy and function of trees—basics and critical developments. *Current Forestry Reports* **2**: 236–248.

Pfautsch S, Harbusch M, Wesolowski A, Smith R, Macfarlane C, Tjoelker MG, Reich PB, Adams MA. 2016. Climate determines vascular traits in the ecologically diverse genus Eucalyptus. *Ecology Letters* **19**: 240–248.

Piggin J, Bruhl JJ. 2010. Phylogeny reconstruction of *Callitris* Vent. (Cupressaceae) and its allies leads to inclusion of *Actinostrobus* within *Callitris*. *Australian Systematic Botany* **23**: 69–93.

Pittermann J, Choat B, Jansen S, Stuart SA, Lynn L, Dawson TE. 2010. The relationships between xylem safety and hydraulic efficiency in the Cupressaceae: the evolution of pit membrane form and function. *Plant Physiology* **153**: 1919–1931.

Pittermann J, Limm E, Rico C, Christman MA. 2011. Structure–function constraints of tracheid-based xylem: a comparison of conifers and ferns. *New Phytologist* **192**: 449–461.

Pittermann J, Sperry JS, Hacke UG, Wheeler JK, Sikkema EH. 2005. Torus-margo pits help conifers compete with angiosperms. *Science* **310**: 1924.

Pittermann J, Sperry JS, Hacke UG, Wheeler JK, Sikkema EH. 2006a. Inter-tracheid pitting and the hydraulic efficiency of conifer wood: the role of tracheid allometry and cavitation protection. *American Journal of Botany* **93**: 1265–1273.

Pittermann J, Sperry JS, Wheeler JK, Hacke UG, Sikkema EH. 2006b. Mechanical reinforcement of tracheids compromises the hydraulic efficiency of conifer xylem. *Plant, Cell & Environment* **29**: 1618–1628.

Pittermann J, Stuart SA, Dawson TE, Moreau A. 2012. Cenozoic climate change shaped the evolutionary ecophysiology of the Cupressaceae conifers. *Proceedings of the National Academy of Sciences, USA* **109**: 9647–9652.

Polge H. 1966. Établissement des courbes de variation de la densité du bois par exploration densitométrique de radiographies d'échantillons prélevés à la tarière

sur des arbres vivants Applications dans les domaines Technologique et Physiologique. *Annales des sciences forestières* **23**: 215.

Poorter L, McDonald I, Alarcón A, Fichtler E, Licona JC, Peña-Claros M, Sterck F, Villegas Z, Sass-Klaassen U. 2010. The importance of wood traits and hydraulic conductance for the performance and life history strategies of 42 rainforest tree species. *New Phytologist* **185**: 481–492.

Pouteau R, Birnbaum P. 2016. Island biodiversity hotspots are getting hotter: vulnerability of tree species to climate change in New Caledonia. *Biological Conservation* **201**: 111–119.

Pouteau R, Trueba S, Feild TS, Isnard S. 2015. New Caledonia: a Pleistocene refugium for rain forest lineages of relict angiosperms. *Journal of Biogeography* **42**: 2062–2077.

Pybus OG, Harvey PH. 2000. Testing macro-evolutionary models using incomplete molecular phylogenies. *Proceedings of the Royal Society of London. Series B, Biological Sciences* **267**: 2267–2272.

Pye MG, Gadek PA, Edwards KJ. 2003. Divergence, diversity and species of the Australasian Callitris (Cupressaceae) and allied genera: evidence from ITS sequence data. *Australian Systematic Botany* **16**: 505–514.

Quantum G. 2011. Development Team, 2012. Quantum GIS Geographic Information System. Open Source Geospatial Foundation Project. [WWW document] URL http://qgis.osgeo.org/en/site/ [accessed 28 February 2017].

Qvarnström A, Ålund M, Mcfarlane SE, Sirkiä PM. 2016. Climate adaptation and speciation: particular focus on reproductive barriers in Ficedula flycatchers. *Evolutionary Applications* **9**: 119–134.

R Core Team. 2015. R: a language and environment for statistical computing 3.12. [WWW document] URL https://www.r-project.org/ [accessed 28 February 2017]

Revell LJ. 2013. Two new graphical methods for mapping trait evolution on phylogenies (R Freckleton, ed.). *Methods in Ecology and Evolution* **4**: 754–759.

Sáenz-Romero C, Lamy J-B, Loya-Rebollar E, Plaza-Aguilar A, Burlett R, Lobit P, Delzon S. 2013. Genetic variation of drought-induced cavitation resistance among *Pinus hartwegii* populations from an altitudinal gradient. *Acta Physiologiae Plantarum* **35**: 2905–2913.

Santiago LS, Goldstein G, Meinzer FC, Fisher JB, Machado K, Woodruff D, Jones T. 2004. Leaf photosynthetic traits scale with hydraulic conductivity and wood density in Panamanian forest canopy trees. *Oecologia* **140**: 543–550.

Sax DF, Early R, Bellemare J. 2013. Niche syndromes, species extinction risks, and management under climate change. *Trends in Ecology & Evolution* **28**: 517–523.

Schuldt B, Knutzen F, Delzon S, Jansen S, Müller-Haubold H, Burlett R, Clough Y, Leuschner C. 2015. How adaptable is the hydraulic system of European beech in the face of climate change-related precipitation reduction? *New Phytologist* **210**: 443–458.

Smith SA, Beaulieu JM, Donoghue MJ. 2009. Mega-phylogeny approach for comparative biology: an alternative to supertree and supermatrix approaches. *BMC Evolutionary Biology* **9**: 37.

Sperry JS. 2003. Evolution of water transport and xylem structure. *International Journal of Plant Sciences* **164**: S115–S127.

Sperry JS, Hacke UG, Pittermann J. 2006. Size and function in conifer tracheids and angiosperm vessels. *American Journal of Botany* **93**: 1490–1500.

Sperry JS, Meinzer FC, McCulloh KA. 2008. Safety and efficiency conflicts in hydraulic architecture: scaling from tissues to trees. *Plant, Cell & Environment* **31**: 632–645.

Stocker TF, Qin D, Plattner G-K, Tignor MM, Allen SK, Boschung J, Nauels A, Xia Y, Bex V, Midgley PM. 2013. IPCC, 2013: Climate change 2013: the physical science basis. In: Stocker TF, Qin D, Plattner G-K, Tignor MM, Allen SK, Boschung J, Nauels A, Xia Y, Bex V, Midgley PM, eds. *Contribution of Working Group I to the Fifth Assessment Report of the Intergovernmental Panel on Climate Change*. Cambridge, UK and New York, NY, USA: Cambridge University Press, 1–1535.

Tamura K, Peterson D, Peterson N, Stecher G, Nei M, Kumar S. 2011. MEGA5: molecular evolutionary genetics analysis using maximum likelihood, evolutionary distance, and maximum parsimony methods. *Molecular Biology and Evolution* **28**: 2731–2739.

Thuiller W, Lavergne S, Roquet C, Boulangeat I, Lafourcade B, Araujo MB. 2011. Consequences of climate change on the tree of life in Europe. *Nature* **470**: 531–534.

Thuiller W, Lavorel S, Araújo MB. 2005. Niche properties and geographical extent as predictors of species sensitivity to climate change. *Global Ecology and Biogeography* **14**: 347–357.

Trabucco A, Zomer RJ. 2009. Global Aridity Index (Global-Aridity) and Global Potential Evapo-Transpiration (Global-PET) Geospatial Database. CGIAR Consortium for Spatial Information. [WWW document] URL http://www.cgiar-csi.org/data/global-aridity-and-pet-database [accessed 28 February 2017].

Tyree MT, Sperry JS. 1989. Vulnerability of xylem to cavitation and embolism. *Annual Review of Plant Biology* **40**: 19–36.

Tyree MT, Zimmermann MH. 2002. *Xylem structure and the ascent of sap*. Berlin, Heidelberg, Germany: Springer Science & Business Media.

Urli M, Porté AJ, Cochard H, Guengant Y, Burlett R, Delzon S. 2013. Xylem embolism threshold for catastrophic hydraulic failure in angiosperm trees. *Tree Physiology* **33**: 672–683.

Wheeler JK, Sperry JS, Hacke UG, Hoang N. 2005. Inter-vessel pitting and cavitation in woody Rosaceae and other vessel led plants: a basis for a safety versus efficiency trade-off in xylem transport. *Plant, Cell and Environment* **28**: 800–812.

Wilf P, Little SA, Iglesias A, Del Carmen Zamaloa M, Gandolfo MA, Cúneo NR, Johnson KR. 2009. Papuacedrus (Cupressaceae) in Eocene Patagonia: a new fossil link to Australasian rainforests. *American Journal of Botany* **96**: 2031–2047.

Willson CJ, Manos PS, Jackson RB. 2008. Hydraulic traits are influenced by phylogenetic history in the drought-resistant, invasive genus *Juniperus* (Cupressaceae). *American Journal of Botany* **95**: 299–314.

Zachos JC, Dickens GR, Zeebe RE. 2008. An early Cenozoic perspective on greenhouse warming and carbon-cycle dynamics. *Nature* **451**: 279–283.

Zachos J, Pagani M, Sloan L, Thomas E, Billups K. 2001. Trends, rhythms, and aberrations in global climate 65 Ma to present. *Science* **292**: 686–693.

Zimmer HC, Brodribb TJ, Delzon S, Baker PJ. 2016. Drought avoidance and vulnerability in the Australian Araucariaceae. *Tree Physiology* **36**: 218–228.

Supporting Information

Additional Supporting Information may be found online in the Supporting Information tab for this article:

Fig. S1 Time-tree from the BEAST analysis using only cpDNA, and only nuclear sequences.

Fig. S2 Tracheid length and number of pits per tracheid against P_{50} and K_s.

Fig. S3 Ancestral trait reconstruction of embolism resistance (P_{50}) in the *Callitris* clade.

Table S1 GenBank accessions for the sequences used in this study, and model parameters specified for the BEAST analysis

Table S2 Trait data for the 23 species studied in this paper

Table S3 Correlation between climate variables and P_{50}, tracheid diameter, and wood density

Table S4 Correlation between hydraulic (P_{50}, K_s) traits, wood density, and xylem traits

Please note: Wiley Blackwell are not responsible for the content or functionality of any Supporting Information supplied by the authors. Any queries (other than missing material) should be directed to the *New Phytologist* Central Office.

***New Phytologist* Supporting Information**

Article title: **Aridity drove the evolution of extreme embolism resistance and the radiation of conifer genus *Callitris***

Authors: **Maximilian Larter, Sebastian Pfautsch, Jean-Christophe Domec, Santiago Trueba, Nathalie Nagalingum and Sylvain Delzon**

Article acceptance date: 26 February 2017

The following Supporting Information is available for this article:

Fig. S1 BEAST and RAxML analyses on nuclear and plastid datasets.

Fig. S2 Tracheid length and number of pits per tracheid against P_{50} and K_s.

Fig. S3 Ancestral trait reconstruction of embolism resistance (P_{50}) in the *Callitris* clade.

Table S1 GenBank accessions for the sequences used in this study, and model parameters specified for the BEAST analysis.

Table S2 Trait data for the 23 species studied in this paper.

Table S3 Correlation between climate variables and P_{50}, tracheid diameter, and wood density.

Table S4 Correlation between hydraulic (P_{50}, K_s) traits, wood density, and xylem traits.

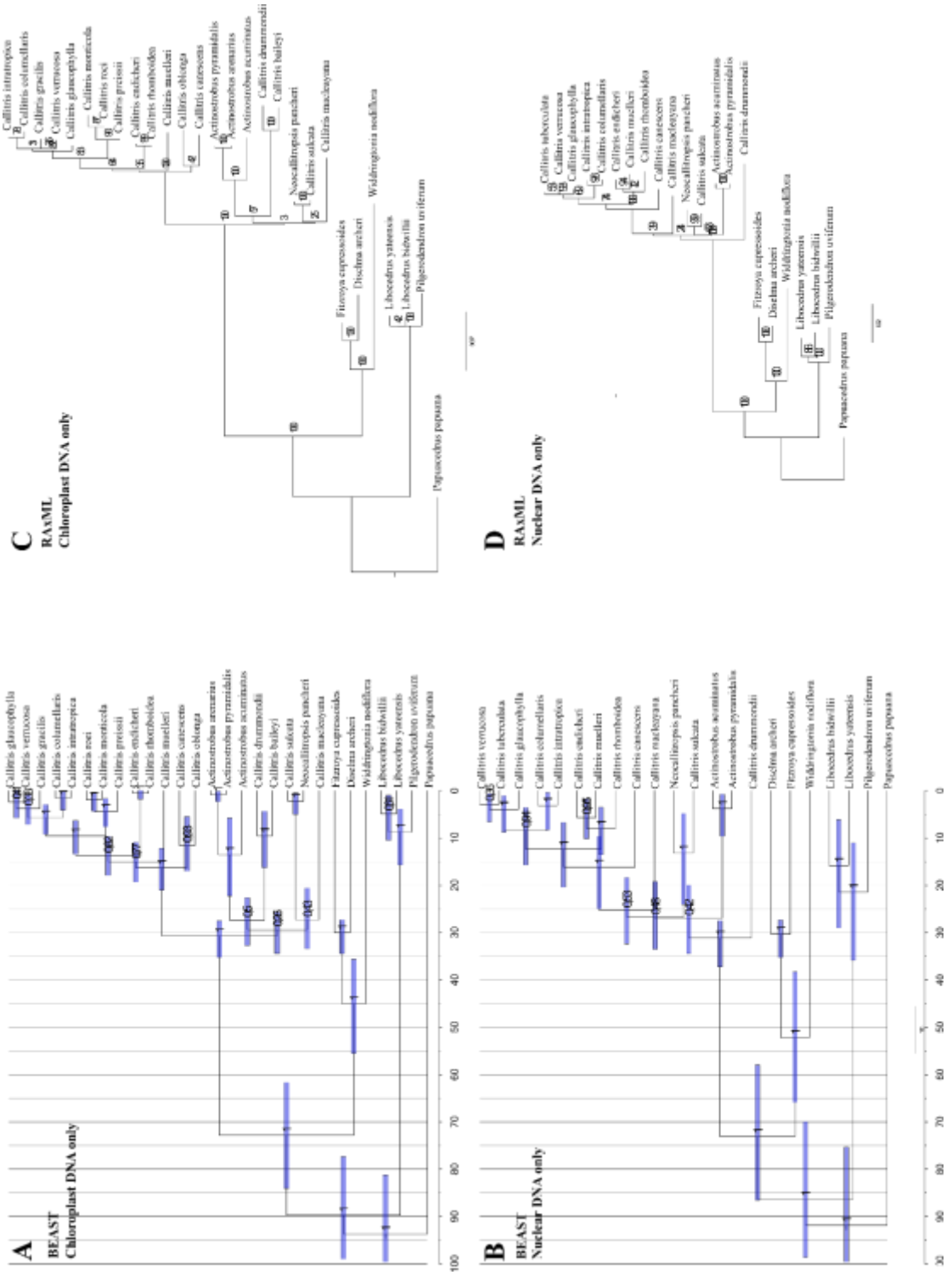

Fig. S1. BEAST and RAxML analyses on nuclear and plastid datasets. Timetrees from the BEAST analysis using (A) only cpDNA and (B) only nuclear sequences, and phylogenetic trees from RAxML using (C) only cpDNA and (D) only nuclear sequences

Figure S2. Tracheid length and number of pits per tracheid against P_{50} and K_s. Partial datasets only. Linear models fit through the data are shown. Linear regression lines are shown, with the adjusted R^2. "*" indicates p-values < 0.05, and "ns" indicates non-significance at α=0.05.

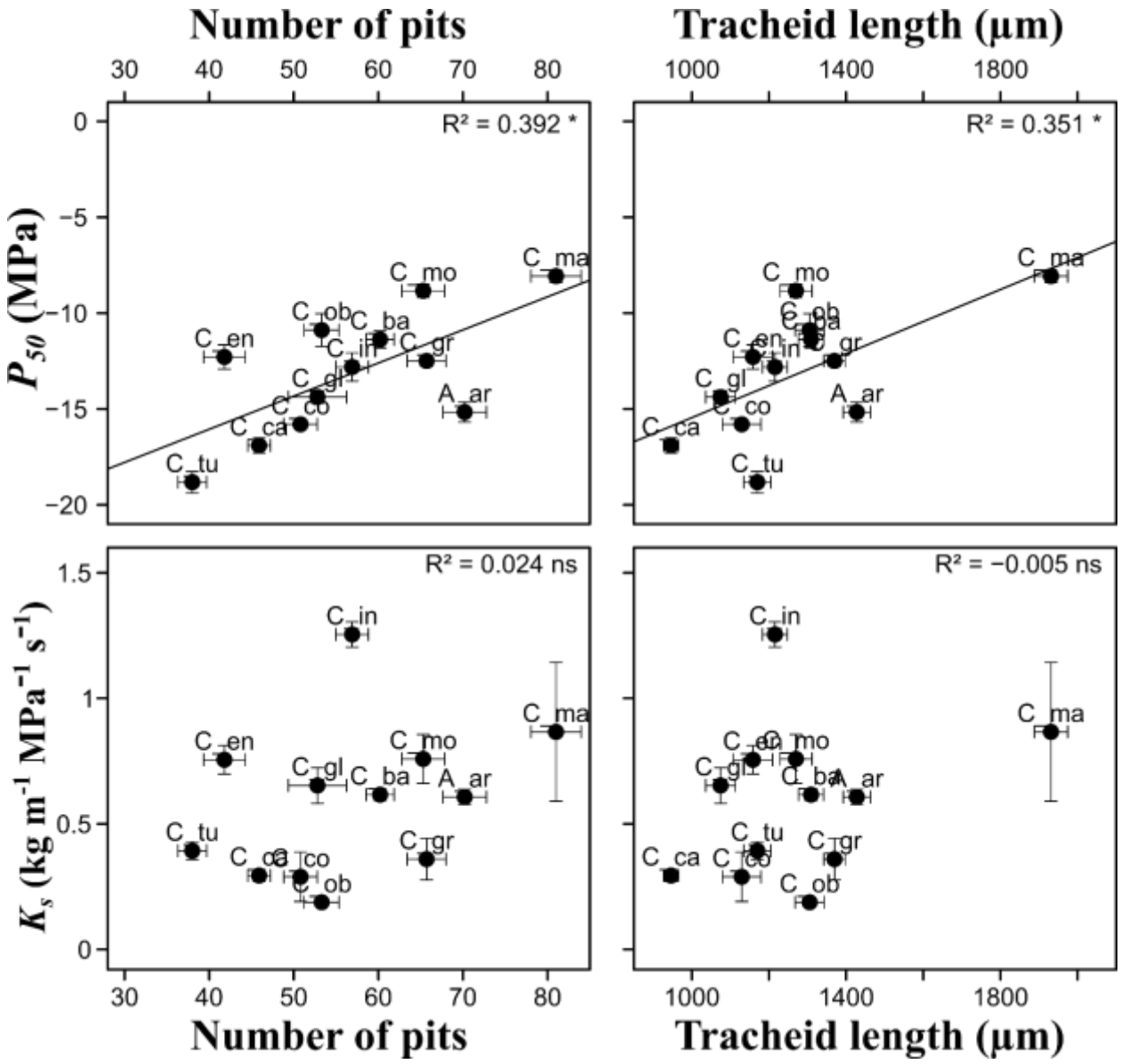

Figure S3. Ancestral trait reconstruction of embolism resistance (P_{50}) in the *Callitris* clade. Node numbers on the phylogeny correspond to node ancestral states in the table, which also contains 95% CI. This analysis used maximum likelihood implemented with the *ace* function of the *ape* package in R.

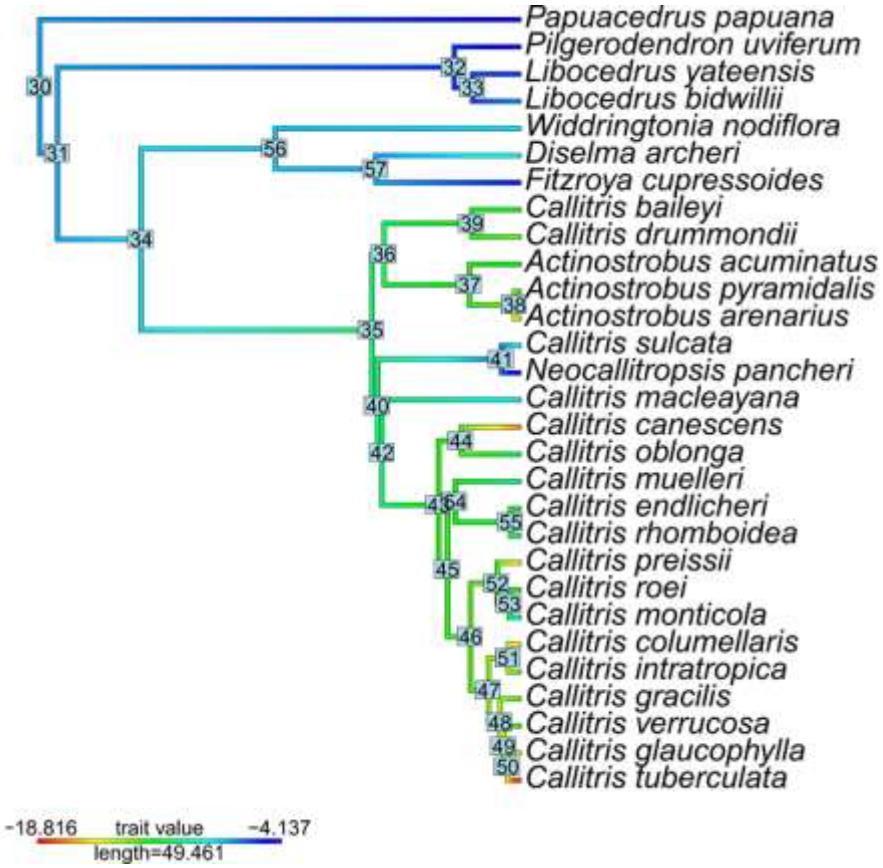

Node number	Ancestral P50	Lower 95% CI	Upper 95% CI
30	-7.02	-12.45	-1.58
31	-7.10	-12.31	-1.89
32	-5.51	-7.97	-3.06
33	-5.74	-7.84	-3.64
34	-7.84	-12.54	-3.15
35	-10.44	-12.92	-7.95
36	-10.79	-13.37	-8.21
37	-12.14	-14.38	-9.90
38	-13.41	-14.13	-12.70
39	-11.93	-14.15	-9.72
40	-10.34	-12.77	-7.91
41	-6.45	-7.87	-5.04
42	-10.40	-12.84	-7.96
43	-12.14	-14.09	-10.20
44	-12.91	-15.00	-10.83
45	-12.11	-13.93	-10.29
46	-12.88	-14.58	-11.17
47	-13.68	-15.10	-12.26
48	-13.89	-15.02	-12.76
49	-14.25	-15.27	-13.24
50	-15.21	-16.17	-14.25
51	-14.18	-15.22	-13.14
52	-12.58	-13.98	-11.19
53	-11.09	-12.09	-10.10
54	-11.83	-13.75	-9.92
55	-11.34	-12.33	-10.35
56	-7.52	-11.82	-3.22
57	-7.14	-10.83	-3.44

Table S1. GenBank accessions for the sequences used in this study, and model parameters specified for the BEAST analysis.

Species	RBCL	MATK	TRNL	ITS1	PSBB	PETB	NEEDLY	LEAFY
Actinostrobus acuminatus		AF152175.1		AY178417.1				
Actinostrobus arenarius	JF725937.1	JF725837.1	JF725897.1		JF725977.1	JF725790.1		
Actinostrobus pyramidalis	JF725931.1	JF725831.1	JF725891.1	AY178415.1	JF725970.1	JF725783.1	HQ245712.1	HQ245806.1
Callitris canescens	JF725945.1	JF725845.1	JF725905.1	AY178411.1	JF725985.1	JF725798.1		
Callitris columellaris			AB723688.1	AY178404.1			HQ245715.1	HQ245809.1
Callitris drummondii	JF725939.1	JF725839.1	JF725899.1	AY178423.1	JF725979.1	JF725792.1		
Callitris endlicheri	JF725932.1	JF725832.1	AY988417.1	AY178425.1	JF725971.1	JF725784.1	AY988419.1	
Callitris glaucophylla	KM895763.1		AB723697.1					
Callitris gracilis			AB723693.1					
Callitris intratropica			AB723690.1	AY178400.1				
Callitris macleayana	JF725933.1	JF725833.1	JF725893.1	AY178421.1	JF725972.1	JF725785.1	HQ245716.1	HQ245810.1
Callitris muelleri	JF725924.1	JF725824.1	JF725884.1	AY178412.1	JF725963.1	JF725776.1		
Callitris oblonga				AY178429.1				
Callitris preissii	JF725940.1	JF725840.1	JF725900.1		JF725980.1	JF725793.1		
Callitris rhomboidea	JF725925.1	JF725825.1	JF725885.1	AY178406.1	JF725964.1	JF725777.1	HQ245717.1	HQ245811.1
Callitris sulcata	JF725941.1	JF725841.1	JF725901.1	AY178422.1	JF725981.1	JF725794.1		
Callitris tuberculata				AY178426.1				
Callitris verrucosa	JF725942.1	JF725842.1	AB723695.1	HM116955.1	JF725982.1	JF725795.1	AY988420.1	
Diselma archeri	JF725926.1	JF725826.1	JF725886.1		JF725965.1	JF725778.1	HQ245730.1	HQ245823.1
Fitzroya cupressoides	JF725916.1	JF725816.1	JF725876.1		JF725955.1	JF725768.1	HQ245732.1	HQ245825.1
Libocedrus bidwillii	JF725927.1	JF725827.1	JF725887.1		JF725966.1	JF725779.1	HQ245746.1	HQ245838.1
Libocedrus yateensis		HQ245902.1					HQ245748.1	HQ245840.1
Neocallitropsis pancheri	JF725934.1	JF725834.1	JF725894.1	AY178420.1	JF725974.1	JF725787.1	HQ245751.1	HQ245843.1
Papuacedrus papuana	JF725935.1	JF725835.1	JF725895.1		JF725975.1	JF725788.1	HQ245752.1	HQ245844.1
Pilgerodendron uviferum	JF725929.1	HQ245907.1	JF725889.1		JF725968.1	JF725781.1	HQ245753.1	HQ245845.1
Widdringtonia nodiflora	JF725930.1	JF725830.1	AY988418.1		JF725969.1	JF725782.1	HQ245766.1	HQ245856.1
Alignment length (nucleotides)	1278	1551	395	1051	1344	1289	3705	2942
Substitution model (BEAST)	HKY+G	HKY+G	HKY	HKY+G	HKY+G	HKY+G	HKY+I	TN93+G

Table S2. Trait data for the 23 species studied in this paper. Abbreviations as follows: N = number of individuals measured for hydraulic traits; P_{50} = xylem pressure inducing 50% loss of hydraulic conductance (MPa); slope = slope of the vulnerability curve (% MPa^{-1}); K_s = xylem specific hydraulic conductance (kg m^{-1} MPa^{-1} s^{-1}); WD = wood density (g cm^{-3}); MeanD, MinD, MaxD = mean, minimum and maximum tracheid diameters respectively (µm); D_s = hydraulically weighted tracheid diameter (µm) calculated as D^5/D^4; D_h = hydraulically weighted diameter (µm) calculated as: $D_h = [\frac{\sum D^4}{N}]^{1/4}$; Vwr = void to wood ratio (%); TF = tracheid frequency (n mm^{-2}); K_{th} = theoretical hydraulic conductance (kg m^{-1} MPa^{-1} s^{-1}) calculated using the Hagen-Poiseuille law; N_tracheids = total number of tracheids measured for each species. Median values over each species distribution for AI = Aridity index, Med_bio1 = annual temperature, Med_bio12 = annual precipitations (mm). Variables starting with SE or ending with e are standard error.

Table S2

Species	P50	slope	Ks	densityMEANcor	densityMEANe	P50e	slopee	Kse	MeanD	Ds	MinD	Max_D	Dh
Actinostrobus_acuminatus	-11,52	15,11	0,438	0,68	0,012	0,75	0,66	0,063	10,86	14,3	3,41	20,78	18,27
Actinostrobus_arenarius	-15,16	11,13	0,606	0,69	0,025	0,52	0,87	0,030	10,26	13,37	3,09	18,86	15,17
Actinostrobus_pyramidalis	-11,78	17,83	0,512	0,58	0,021	0,36	1,29	0,045	9,26	12,3	2,85	17,19	15,74
Callitris_baileyi	-11,37	20,35	0,615	0,56	0,004	0,44	0,58	0,023	11,31	13,99	3,56	19,92	12,4
Callitris_canescens	-16,90	9,87	0,294	0,70	0,017	0,40	0,62	0,024	9,08	11,39	2,93	15,89	13,68
Callitris_columellaris	-15,80	15,23	0,289	0,66	0,033	0,18	2,62	0,098	11,27	13,16	4,46	18,34	12,03
Callitris_drummondii	-13,11	18,16	0,477	0,62	0,031	0,28	0,99	0,033	10,15	12,3	3,24	17,17	16,47
Callitris_endlicheri	-12,28	17,58	0,754	0,66	0,008	0,63	2,01	0,056	13,18	16,37	4,43	23,21	14,51
Callitris_glaucophylla	-14,37	19,81	0,652	0,74	0,029	0,33	1,30	0,071	11,02	13,37	3,93	18,99	15,16
Callitris_gracilis	-12,49	19,54	0,359	0,61	0,010	0,28	1,27	0,083	10,37	12,68	3,93	18,07	11,29
Callitris_intratropica	-12,81	14,24	1,252	0,62	0,011	0,73	1,75	0,050	13,22	15,6	4,87	21,86	14,2
Callitris_macleayana	-8,07	27,22	0,865	0,60	0,025	0,33	3,58	0,276	15,91	20,31	5,01	28,54	17,72
Callitris_monticola	-8,84	18,52	0,757	0,50	0,018	0,34	1,62	0,098	13,96	16,03	6,38	22,11	14,78
Callitris_muelleri	-10,10	20,46	0,571	0,47	0,001	0,49	1,45	0,075	10,22	12,54	3	18,67	16,69
Callitris_neocaledonica	-3,83	50,67	0,545	0,69	0,035	0,12	7,80	0,046	13,57	17,31	2,97	26,03	22,5
Callitris_oblonga	-10,88	17,09	0,187	0,57	0,020	0,85	2,13	0,014	12,71	14,58	5,08	19,83	13,47
Callitris_preissii	-14,97	15,56	0,311	0,65	0,013	0,50	2,02	0,062	12,56	14,78	4,65	20,44	13,48
Callitris_rhomboidea	-10,32	27,46	0,257	0,61	0,040	0,53	5,64	0,060	13,66	15,57	5,57	21,5	14,44
Callitris_roei	-12,21	12,37	0,340	0,67	0,017	0,34	0,90	0,020	9,73	12,9	3,39	19,96	16,35
Callitris_sulcata	-8,24	17,91	0,557	0,68	0,018	0,45	1,75	0,043	14,14	18,82	3,82	26,61	24,12
Callitris_tuberculata	-18,82	13,99	0,392	0,72	0,021	0,56	1,16	0,035	9,04	11,27	3,28	15,42	12,85
Callitris_verrucosa	-11,92	18,30	0,521	0,62	0,019	0,17	2,22	0,082	9,87	12,45	3,32	17,6	16,3
Neocallitropsis_pancheri	-4,14	46,58	0,467	0,74	0,037	0,10	4,84	0,036	13,16	18,92	3,47	26,23	23,3

Table S2 (continued)

Species	Void_wood_ratio	Av_tr_mm2	Kth	meanD_SE	Ds_SE	MinD_SE	Max_D_SE	Dh_SE	Void_wood_ratio_SE	Kpit
Actinostrobus_acuminatus	27,12	2686	7,3264	0,17	0,78	0,57	2,59	0,52	0,2	0,47
Actinostrobus_arenarius	24,48	2736	4,6111	0,52	0,61	0,21	0,67	1,99	1,31	0,70
Actinostrobus_pyramidalis	23	3096	4,6715	0,26	0,54	0,41	0,87	0,51	0,87	0,57
Callitris_baileyi	29,78	2820	1,6658	1,13	0,94	0,15	1,09	1,06	2,88	0,98
Callitris_canescens	23,33	3454	3,2284	0,53	0,54	0,28	0,57	0,98	1,14	0,32
Callitris_columellaris	25,14	2403	1,2307	0,2	0,11	0,42	0,92	0,11	0,96	0,38
Callitris_drummondii	28,82	3352	6,0563	0,35	0,22	0,4	0,36	0,42	1,6	0,52
Callitris_endlicheri	35,49	2418	2,6455	0,35	0,73	0,38	1,62	0,5	1,64	1,05
Callitris_glaucophylla	27	2683	4,6733	0,44	0,53	0,14	0,57	1,86	1,34	0,76
Callitris_gracilis	25,92	2880	1,1517	0,26	0,38	0,04	0,83	0,29	2,1	0,52
Callitris_intratropica	25,96	1802	1,7954	0,5	0,67	0,07	1,93	0,57	1,42	4,14
Callitris_macleayana	29,39	1378	3,3503	1,16	0,95	0,64	0,58	1,13	1,88	1,17
Callitris_monticola	34,11	2151	2,5273	0,62	0,71	0,43	1,29	0,67	1,37	1,08
Callitris_muelleri	27,72	3196	6,0500	0,62	0,42	0,45	0,62	0,8	1,6	0,63
Callitris_neocaledonica	25,77	1654	10,6285	0,87	0,99	1,26	1,76	1,38	2,57	0,57
Callitris_oblonga	38,79	2935	2,3606	0,22	0,37	0,18	0,64	0,27	0,36	0,20
Callitris_preissii	31,92	2484	2,0012	0,82	1,03	0,7	1,39	0,86	1,51	0,37
Callitris_rhomboidea	38,7	2603	2,7685	1,13	1,27	0,55	1,33	1,2	1,59	0,28
Callitris_roei	23,77	2938	5,1454	0,23	0,23	0,22	0,88	0,35	0,63	0,36
Callitris_sulcata	27,67	1607	13,2146	0,77	0,86	0,17	1,14	1,21	1,81	0,58
Callitris_tuberculata	22,41	3250	2,4961	0,23	0,38	0,32	0,73	1,11	1,06	0,47
Callitris_verrucosa	24,27	3048	5,1695	0,75	0,91	0,91	1,27	1,2	0,98	0,58
Neocallitropsis_pancheri	24,46	1568	11,5637	0,7	0,95	0,14	1,65	1,18	2,27	0,49

Table S2 (continued)

Species	Av_tr_mm2_SE	Kth_SE	Total_analysed_trach	Med_AI	Med_bio1	Med_bio12	SE_AI	SE_bio1	SE_bio12
Actinostrobus_acuminatus	106	0,54900	798	0,39	18,5	576	0,012	0,11	13,42
Actinostrobus_arenarius	140	1,56221	1782	0,26	19,15	408,5	0,008	0,12	10,65
Actinostrobus_pyramidalis	137	0,48689	920	0,48	18,2	698	0,018	0,17	22,49
Callitris_baileyi	288	0,42884	1447	0,59	18,1	878	0,020	0,20	20,95
Callitris_canescens	264	0,70475	3210	0,28	16,5	372	0,005	0,04	3,87
Callitris_columellaris	18	0,05468	822	0,22	19,6	367	0,018	0,14	22,92
Callitris_drummondii	137	0,56467	996	0,37	16,6	495	0,007	0,05	8,14
Callitris_endlicheri	34	0,33601	1241	0,49	15,7	696	0,004	0,05	4,22
Callitris_glaucophylla	121	1,62207	2224	0,32	17,2	459	0,002	0,03	2,53
Callitris_gracilis	181	0,13888	1478	0,32	15,8	421	0,003	0,03	3,74
Callitris_intratropica	141	0,21095	925	0,69	26,8	1232,5	0,005	0,03	6,78
Callitris_macleayana	105	0,60180	707	1,32	17,7	1690	0,031	0,19	37,04
Callitris_monticola	120	0,31889	1104	0,94	14,25	1220	0,022	0,21	27,14
Callitris_muelleri	287	0,75820	1640	1,07	13,9	1233	0,016	0,18	14,70
Callitris_neocaledonica	104	2,10713	1960	2,03	18,3	2320	0,041	0,28	34,39
Callitris_oblonga	118	0,10134	1506	0,80	12,8	918	0,014	0,09	18,65
Callitris_preissii	268	0,30830	1275	0,26	17	363	0,008	0,07	9,41
Callitris_rhomboidea	299	0,58665	1336	0,83	14,6	924	0,012	0,10	15,00
Callitris_roei	66	0,33899	873	0,29	16,2	387	0,005	0,05	5,24
Callitris_sulcata	178	1,67893	1904	0,98	22,5	1252	0,026	0,14	29,23
Callitris_tuberculata	126	0,67797	2082	0,21	17,3	304	0,007	0,09	6,99
Callitris_verrucosa	487	0,87781	1564	0,25	16,3	345	0,002	0,03	1,92
Neocallitropsis_pancheri	50	2,22655	1858	1,79	21,5	2162	0,024	0,16	27,00

Table S3 Correlation between climate variables and P_{50}, K_s, hydraulically weighted tracheid diameter (D_h), and wood density (WD). We tested correlations with the mean and the median of species climate distributions, and log transformed data (on the medians), and correcting for phylogenetic relatedness using PGLS. R^2 is the adjusted coefficient of determination, p is the p-value at α=0.05 and statistical significance (sig) is indicated by asterisks: *** = p <0.001, ** = p < 0.01, * = p < 0.05, and "ns" indicates non-significance. Relationships that change using climate mean, log-transformation or PGLS are underlined and colored red, and significant relationships are in bold font.

		Median			Mean			Log transformed			PGLS			
		R^2	p	sig	R^2	p	sig	R^2	p	sig	lambda	R^2	p	sig
P_{50}	Mean Annual Rainfall	**0,7833**	**0,000**	***	**0,761**	**0,000**	***	**0,732**	**0,000**	***	**0,000**	**0,806**	**0,001**	***
	Aridity Index	**0,8055**	**0,000**	***	**0,788**	**0,000**	***	**0,769**	**0,000**	***	**0,000**	**0,929**	**0,000**	***
	Mean Annual Temperature	-0,0396	0,692	ns	-0,046	0,877	ns	-0,027	0,519	ns	0,928	-0,054	0,466	ns
K_s	Mean Annual Rainfall	0,0863	0,094	ns	0,065	0,127	ns	0,119	0,060	ns	0,000	-0,082	0,551	ns
	Aridity Index	0,0075	0,292	ns	-0,009	0,378	ns	0,047	0,163	ns	0,000	-0,142	0,958	ns
	Mean Annual Temperature	0,2455	0,009	**	0,261	0,007	ns	0,185	0,023	*	0,000	0,480	0,023	*
D_h	Mean Annual Rainfall	**0,4553**	**0,000**	***	**0,429**	**0,000**	***	**0,344**	**0,002**	**	**0,000**	**0,739**	**0,002**	**
	Aridity Index	**0,4761**	**0,000**	***	**0,451**	**0,000**	***	**0,360**	**0,001**	**	**0,000**	**0,766**	**0,001**	**
	Mean Annual Temperature	0,0827	0,099	ns	0,047	0,164	ns	0,070	0,118	ns	1,000	0,186	0,136	ns
WD	Mean Annual Rainfall	-0,0418	0,7362	ns	-0,0430	0,7637	ns	0,022	0,234	ns	0,000	0,140	0,114	ns
	Aridity Index	-0,0426	0,7547	ns	-0,0428	0,7580	ns	0,032	0,204	ns	0,000	0,197	0,072	ns
	Mean Annual Temperature	0,1354	0,0472	*	0,1101	0,0674	ns	0,197	0,019	*	0,000	-0,036	0,461	ns

Table S4 Correlation between hydraulic (P_{50}, K_s) traits, wood density, and xylem traits (D_h, void to wood ratio, Tracheid frequency and theoretical conductivity). We tested correlations with log transformed data, and correcting for phylogenetic relatedness using PGLS. R^2 is the adjusted coefficient of determination, p is the p-value at α=0.05 and statistical significance (sig) is indicated by asterisks: *** = p <0.001, ** = p < 0.01, * = p < 0.05, and "ns" indicates non-significance. Relationships that change using log-transformation or PGLS are underlined and colored red, and significant relationships are in bold font.

		Linear models			Log transformed			PGLS			
		R^2	p	sig	R^2	p	sig	lambda	R^2	p	sig
***P*$_{50}$**	k_s	-0,0061	0,362	ns	-0,006	0,361	ns	0,000	-0,138	0,864	ns
	Wood density	-0,0888	0,574	ns	-0,011	0,372	ns	0,000	-0,089	0,574	ns
	Dh	**0,5323**	**0,000**	***	**0,554**	**0,000**	***	**0,000**	**0,663**	**0,005**	**
	Void to wood ratio	-0,0009	0,333	ns	-0,037	0,646	ns	1,000	-0,102	0,626	ns
	Tracheid Frequency	**0,4142**	**0,001**	***	**0,464**	**0,000**	***	0,000	0,137	0,176	ns
	Kth	**0,3667**	**0,001**	**	**0,303**	**0,004**	**	**0,000**	**0,629**	**0,007**	**
***K*$_s$**	Wood density	-0,1037	0,633	ns	0,038	0,289	ns	0,000	-0,104	0,633	ns
	Dh	-0,0293	0,548	ns	0,029	0,212	ns	1,000	0,156	0,160	ns
	Void to wood ratio	-0,0433	0,770	ns	-0,029	0,544	ns	1,000	-0,083	0,553	ns
	Tracheid Frequency	**0,2036**	**0,018**	*	**0,173**	**0,028**	*	**1,000**	**0,626**	**0,007**	**
	Kth	-0,0474	0,953	ns	-0,023	0,483	ns	1,000	-0,098	0,607	ns
Dh	Wood density	0,3523	0,054	ns	0,331	0,061	ns	0,000	0,352	0,054	ns
	Void to wood ratio	-0,0133	0,409	ns	-0,024	0,494	ns	1,000	-0,133	0,815	ns
	Tracheid Frequency	**0,3007**	**0,004**	**	**0,310**	**0,003**	**	**0,000**	**0,449**	**0,029**	*
	Kth	**0,9240**	**0,000**	***	**0,866**	**0,000**	***	**0,000**	**0,952**	**0,000**	***